OPEN ACCESS

Geology ARTICLE

The Innovation Geoscience

A low-latitude framework for climate variability over the last 60,000 years

Hai Cheng,[1,2,*] Xiyu Dong,[1] Hanying Li,[1] Xiaowen Niu,[1] Baoyun Zong,[1] Xu Zhang,[3] Xue Jia,[1] Le Kang,[1] Jian Wang,[1] Jingyao Zhao,[1] Kexin Wang,[1] Lijuan Sha,[1] Liang Yi,[4] Ashish Sinha,[1,2,5] Zhengguo Shi,[1,6] Zhifeng Zhang,[7] Yanjun Cai,[1] Haiwei Zhang,[1] Youwei Li,[1] Carlos Pérez-Mejías,[1] Gayatri Kathayat,[1,6] Youfeng Ning,[1] Dianbing Liu,[8] Shitao Chen,[8] Yongjin Wang,[8] Pingzhong Zhang,[9] Francisco W. Cruz,[10] Nicolás M. Stríkis,[10] Xianfeng Wang,[11] Christoph Spötl,[12] and R. Lawrence Edwards[13]

*Correspondence: cheng021@xjtu.edu.cn

Received: May 15, 2026; Accepted: June 29, 2026; Published Online: June 30, 2026; https://doi.org/10.59717/j.xinn-geo.2026.100243

GRAPHICAL ABSTRACT

PUBLIC SUMMARY

- A new high-resolution and precisely dated Asian composite cave record covers past 60,000 years.
- The record's precise chronology provides benchmarks for calibrating and correlating global climate variability.
- The monsoon dynamics were coupled with the Atlantic Meridional Overturning Circulation instead of ice volume.
- The most prominent millennial cycle is ~4.5-ka, close to ¼ precession cycles, implying an external forcing.
- Multidecadal-centennial climate variations in periodicity and amplitude changed from glacial to interglacial.

ARTICLE Geology

OPEN ACCESS

A low-latitude framework for climate variability over the last 60,000 years

Hai Cheng,[1,2,*] Xiyu Dong,[1] Hanying Li,[1] Xiaowen Niu,[1] Baoyun Zong,[1] Xu Zhang,[3] Xue Jia,[1] Le Kang,[1] Jian Wang,[1] Jingyao Zhao,[1] Kexin Wang,[1] Lijuan Sha,[1] Liang Yi,[4] Ashish Sinha,[1,2,5] Zhengguo Shi,[1,6] Zhifeng Zhang,[7] Yanjun Cai,[1] Haiwei Zhang,[1] Youwei Li,[1] Carlos Pérez-Mejías,[1] Gayatri Kathayat,[1,6] Youfeng Ning,[1] Dianbing Liu,[8] Shitao Chen,[8] Yongjin Wang,[8] Pingzhong Zhang,[9] Francisco W. Cruz,[10] Nicolás M. Stríkis,[10] Xianfeng Wang,[11] Christoph Spötl,[12] and R. Lawrence Edwards[13]

[1]Institute of Global Environmental Change, Xi'an Jiaotong University, Xi'an 710049, China

[2]Yunnan Key Laboratory of Plateau Geographical Processes & environmental changes, Faculty of Geography, Yunnan Normal University, Kunming 650500, China

[3]Ice Dynamics and Palaeoclimate, British Antarctic Survey, Cambridge CB3 0ET, United Kingdom

[4]State Key Laboratory of Marine Geology, Tongji University, Shanghai 200092, China

[5]Department of Earth Sciences, California State University, Dominguez Hills, Carson CA 90747, USA

[6]State Key Laboratory of Loess Science, Institute of Earth Environment, Chinese Academy of Sciences, Xi'an 710061, China

[7]State Key Laboratory of Biogeology and Environmental Geology, School of Earth Sciences and Resources, China University of Geosciences, Beijing 100083, China

[8]Key Laboratory of Virtual Geographic Environment, Nanjing Normal University, Nanjing 210023, China

[9]Key Laboratory of Mineral Resources in Western China (Gansu Province), School of Earth Sciences, Lanzhou University, Lanzhou 730000, China

[10]Instituto de Geociências, Universidade de São Paulo, São Paulo-SP CEP 05508-080, Brazil

[11]Earth Observatory of Singapore, Nanyang Technological University, Singapore 637616, Singapore

[12]Institute of Geology, University of Innsbruck, Innrain 52, Innsbruck 6020, Austria

[13]Department of Earth and Environmental Sciences, University of Minnesota, Minneapolis, MN 55455, USA

*Correspondence: cheng021@xjtu.edu.cn

Received: May 15, 2026; Accepted: June 29, 2026; Published Online: June 30, 2026; https://doi.org/10.59717/j.xinn-geo.2026.100243

Citation: Cheng H., Dong X., Li H., et al. (2026). A low-latitude framework for climate variability over the last 60,000 years. *The Innovation Geoscience* **4**:100243.

Climate variability during the last 60,000 years exhibited pronounced fluctuations on glacial-interglacial to sub-orbital timescales, yet fundamental questions remain regarding the timing, phasing, and cyclical structure of global climate fluctuations. Here we present ASM-2026, a composite of multiple high-resolution speleothem oxygen isotope ($\delta^{18}O$) records from the Asian summer monsoon (ASM) domain spanning the last 60 ka. Anchored by a rigorously constrained U-Th chronology (XJTU-1.0), this record resolves monsoon variability at multidecadal to millennial scales and provides robust geochronological benchmarks for correlating inter-regional climate variability. Our analysis indicates that ASM dynamic variability is only weakly linked to high-latitude ice-sheet forcing in either hemisphere, but closely tracks changes in the Atlantic Meridional Overturning Circulation (AMOC). Terminations of Heinrich Stadials are consistently preceded by centennial-scale weakening of the South American monsoon, likely associated with a shift in the Antarctic Oscillation from positive to negative phase, implicating a low-latitude and/or Southern Hemisphere trigger for abrupt climate reorganization. The record contains pronounced ~4.5-ka cycle close to one-quarter of the precession period, consistent with the modulation by the equatorial insolation forcing. At multidecadal to centennial timescales, the amplitude and periodicity of variability in the ASM and Greenland climate records diminish from glacial to interglacial conditions, whereas Antarctic variability displays an opposing response, highlighting a fundamental reorganization of teleconnections and forcing pathways across climate states.

INTRODUCTION

The climate variability over the past ~60 ka (thousand years) was characterized by a change from the last glacial, through the deglaciation, to the current interglacial period (Holocene). Superimposed on this glacial-interglacial variation are prominent climate oscillations on millennial timescales, including the Dansgaard-Oeschger (DO) events during the last glacial, the Younger Dryas (YD) and Heinrich Stadial 1 (HS1) during the deglaciation (~19–11.7 ka BP, before present, where present is 1950 CE), and the 8.2 ka event in the Holocene (~11.7 ka BP to present).[1,2] Each DO event, as manifested in Greenland ice-core oxygen isotope ($\delta^{18}O$) records, commenced with a rapid transition to a warm state, known as the onset of Greenland Interstadials (GIs), followed by a gradual and then abrupt return to a cold state, the Greenland Stadials (GSs).[2] Besides, Heinrich events (HEs), characterized by layers of ice-rafted debris (IRD) in North Atlantic sediment cores, represent periods of massive iceberg discharges into the North Atlantic.[3,4] The North Atlantic cold phases that span HEs are defined as Heinrich Stadials (HSs),[5,6] noting that HSs often refer to the late phase of the corresponding GSs.[7]

GSs, HSs, the YD, and the 8.2 ka event were of global extent and impact.[8-10] Much across the Northern Hemisphere (NH), these events generally manifested in cooler/drier conditions concomitant with southward displacements of the Intertropical Convergence Zone (ITCZ)[11,12] and the mid-latitude Westerlies.[13] In the Asian summer monsoon (ASM) domain, these events were associated with weakened summer monsoon intensity/convection (namely Chinese Stadials, CSs).[7,14-16] In contrast, many regions in the Southern Hemisphere (SH), especially the South American monsoon (SAM) domain, generally became wetter during these periods (hereafter referred to as South American pluvial periods).[12,17-21] Meanwhile, Antarctica experienced a warming due to heat accumulation in the Southern Ocean[22] as a consequence of reduced northward heat transport from the SH to the NH via the Atlantic meridional overturning circulation (AMOC)[23] and the southward shift of the SH Westerlies[24,25]—an essential aspect of the global thermal 'bipolar-seesaw'.[22,24,26-28]

Over the past half century, extensive proxy and modeling studies have significantly contributed to an improved understanding of climate variations on a wide range of timescales over the last 60 ka. A key mechanism involves changes in the AMOC and its cascading effects, which is causally linked to the North Atlantic freshwater forcing, as a part of spontaneous oscillation.[2,5-7,9,10,15,16,27,29] However, comprehensive characterization of prevailing cycles at various timescales and precise correlation among climate variabilities across the globe remain incomplete. This is especially true for high- and low-latitude climate oscillations, primarily due to the lack of precisely dated climate records and causally explicit correlation strategies, which hinders our ability to further understand a number of outstanding issues in the field.

Over the past two decades, major refinements in U-Th dating techniques (e.g., ref.[30]) have resulted in the development of a new-generation of cave $\delta^{18}O$ records from ASM regions that are characterized by high temporal resolution and precise age control (e.g., refs.[7,9,15,16,31-33]). On the other forefront, a consensus is steadily emerging on the interpretation of ASM cave $\delta^{18}O$ records—primarily indicating ASM dynamics or circulation/convection.[34,35] In this study, we report a new composite cave $\delta^{18}O$ record from the ASM domain over the last 60 ka. By precisely constraining timings of abrupt climate shifts in the record we developed a set of precise chronological benchmarks for correlating and calibrating global climate variability. On the basis of sensible strategies for correlating cave, marine, and ice-core records, we established a coherent chronology of climate variability for the last 60 ka, which provides a compelling framework to decipher a number of outstanding

Table 1. Detailed information of the ASM-2026 record.

Time interval (Years BP)	Cave-speleothem name	Changes of the absolute value of $\delta^{18}O$	References
−50 to 8,800	Dongge Cave-DA	None	Ref.[41]
8,990 to 10,570	Dongge Cave-D4	None	Ref.[42]
10,600 to 11,120	Hulu Cave-H82	None	Ref.[40]
11,130 to 13,070	Shennong Cave-SN29	−1.7‰	Ref.[9]
13,070 to14,440	Hulu Cave-H82	None	Ref.[40]
14,440 to 18,330	Hulu Cave-YT	None	Ref.[43]
18,330 to 19,250	Hulu Cave-H82	None	Ref.[40]
19,260 to 53,060	Hulu Cave-MSD	None	Isotope: this study; U-Th dates: ref.[40]
53,060 to 54,650	Wulu Cave-Wu26	+1.93‰	Isotope: ref.[44]; U-Th dates: this study
54,650 to 57,830	Shennong Cave-SN23-1	−1.1‰	Ref.[16]
57,840 to 60,650	Wulu Cave-Wu23	+1.93‰	Isotope: ref.[44]; U-Th dates: this study

issues in climate variability over this critical period. Specifically, our work sheds light on the relationship between low-latitude monsoons and high-latitude AMOC, the causes and global propagation directionality of millennial-scale climate changes, and multiple-scale climate cycles throughout the last 60 ka.

MATERIALS AND METHODS

U-Th dating

A total of 177 ^{230}Th-dating subsamples were drilled from the polished slabs of stalagmites using carbide dental burrs with a diameter of 0.3 mm. The dating work was performed at the Isotope Laboratory, Xi'an Jiaotong University, China, using multi-collector inductively coupled plasma mass spectrometers (MC-ICP-MS) (Thermo-Finnigan Neptune-*plus*). We used standard chemistry procedures to separate U and Th.[36] A triple-spike (^{229}Th-^{233}U-^{236}U) isotope dilution method was employed to correct for instrumental fractionation and determine U-Th isotopic ratios and concentrations. The instrumentation, standardization and half-lives are reported in refs.[30,37]. All U-Th isotopes were measured on a MasCom multiplier behind the retarding potential quadrupole in the peak-jumping mode. We followed similar procedures of characterizing the multiplier as described in ref.[37]. Uncertainties in U-Th isotopic data were calculated offline at 2σ level, including corrections for blanks, multiplier dark noise, abundance sensitivity, and contents of the same nuclides in spike solution. Corrected ^{230}Th ages assume an initial ^{230}Th/^{232}Th atomic ratio of (4.4 ± 2.2) x10^{-6}, i.e., value for a material at secular equilibrium with the bulk earth ^{232}Th/^{238}U value of 3.8. The dating results are listed in Data S1.

Age models

Age models were calculated using the StalAge software.[38] The StalAge algorithm is based on two assumptions: (1) the age model is monotonic, and (2) a straight line is fitted through as many data points as possible within error bars.[38] Through Monte-Carlo simulation, StalAge generates 300 realizations of age models to account for the 95% confidence limits.[38] Major outliers are detected by disagreement with at least two data points, while minor outliers are screened if more than 80% of the simulated straight lines fail to have a positive slope. In our study, we did not identify any major or minor outliers, as all ages in each age model increased monotonically within dating uncertainties (Figure S1).

The chronological framework for the Hulu Cave (Figure S2) speleothem MSD was previously constructed using the OxCal modeling software (Figure S3).[39,40] This study generated ~3800 new high-resolution $\delta^{18}O$ data from the MSD, and the existing age model required only minor refinements to accord with the targeted age 'spikes', as discussed in the section "The ASM-2026 record over the last 60 ka on the XJTU-1.0 chronology".

Stable isotope analyses

For each oxygen isotope measurement of the sample MSD, ~100 μg of powder was drilled. A total of ~3800 subsamples were micromilled at 0.1 mm increments perpendicularly to the growth axis and analyzed using a Thermo Scientific MAT253-*plus* mass spectrometer coupled with an on-line carbonate preparation device (Kiel-IV) at the Isotope Laboratory, Xi'an Jiaotong University. The analytical error (1σ) is generally 0.06‰ and 0.03‰ for $\delta^{18}O$ and $\delta^{13}C$, respectively. The international standards TTB1 and NBS18 were added to the analysis for every 15 samples to check for reproducibility. Results are reported relative to the Vienna Pee Dee Belemnite (VPDB) standard.

The ASM-2026 record over the last 60 ka on the XJTU-1.0 chronology

In this study, we constructed a new high-resolution composite cave $\delta^{18}O$ record, termed ASM-2026 (Data S2) on a more precise chronology, termed XJTU-1.0, by integrating multiple speleothem datasets from the ASM domain. To ensure a high-quality synthesis, we selected records that offer both high resolution and robust chronological constraints. The composite record primarily incorporates speleothem dataset from Hulu Cave (H82, YT, and MSD) spanning a major portion of the last glacial period to the early Holocene (53.06–10.6 ka BP), while Holocene period predominantly relies on Dongge Cave records (DA and D4), and the older portion of the last glacial mainly on Wulu (Wu23 and Wu26) and Shennong (SN23-1) cave records (Table 1).

The selection of the Hulu YT record for the interval 18.3–14.4 ka BP is justified by its annually laminated structure and high temporal resolution,[43,45] which enables precise chronological alignments of the abrupt monsoon transitions during the last glacial termination. To extend the composite record into the early Holocene (13.07–11.13 ka BP), we integrated the Shennong Cave SN29 $\delta^{18}O$ time series (with an offset-adjustment of −1.7‰), a high-precision dataset covering the full YD event.[9]

For the old portion of ASM-2026 (60.65–57.84 ka BP), we utilized the $\delta^{18}O$ time series from Wulu Cave speleothems (Wu26 and Wu23)[44] (with an offset-adjustment of +1.93‰). These archives preserve centennial- to millennial-scale monsoon variability during the late MIS 4 and the early MIS 3, with chronological refinements achieved through new obtained U-Th dates (Figure S1). The temporal gap between 57.83 and 54.65 ka BP was bridged using the Shennong Cave SN23-1 record[16] (with an offset-adjustment of −1.1 ‰), which uniquely resolves the short-lived CI-15.1 event (~100-year duration). The offsets were corrected by applying a constant shift based on the mean $\delta^{18}O$-value difference over overlapping periods. This linear adjustment aligns the absolute values into a unified baseline while strictly preserving the original high-frequency climatic variability of each record.

The Hulu cave MSD record covers the longest time interval (53.06–19.26 ka BP) in the ASM-2026 record. A previous study[40] has established an age model for the MSD record, and in this study, we obtained a higher resolution (~8 years) $\delta^{18}O$ dataset with an improved age model. The key geochronologi-

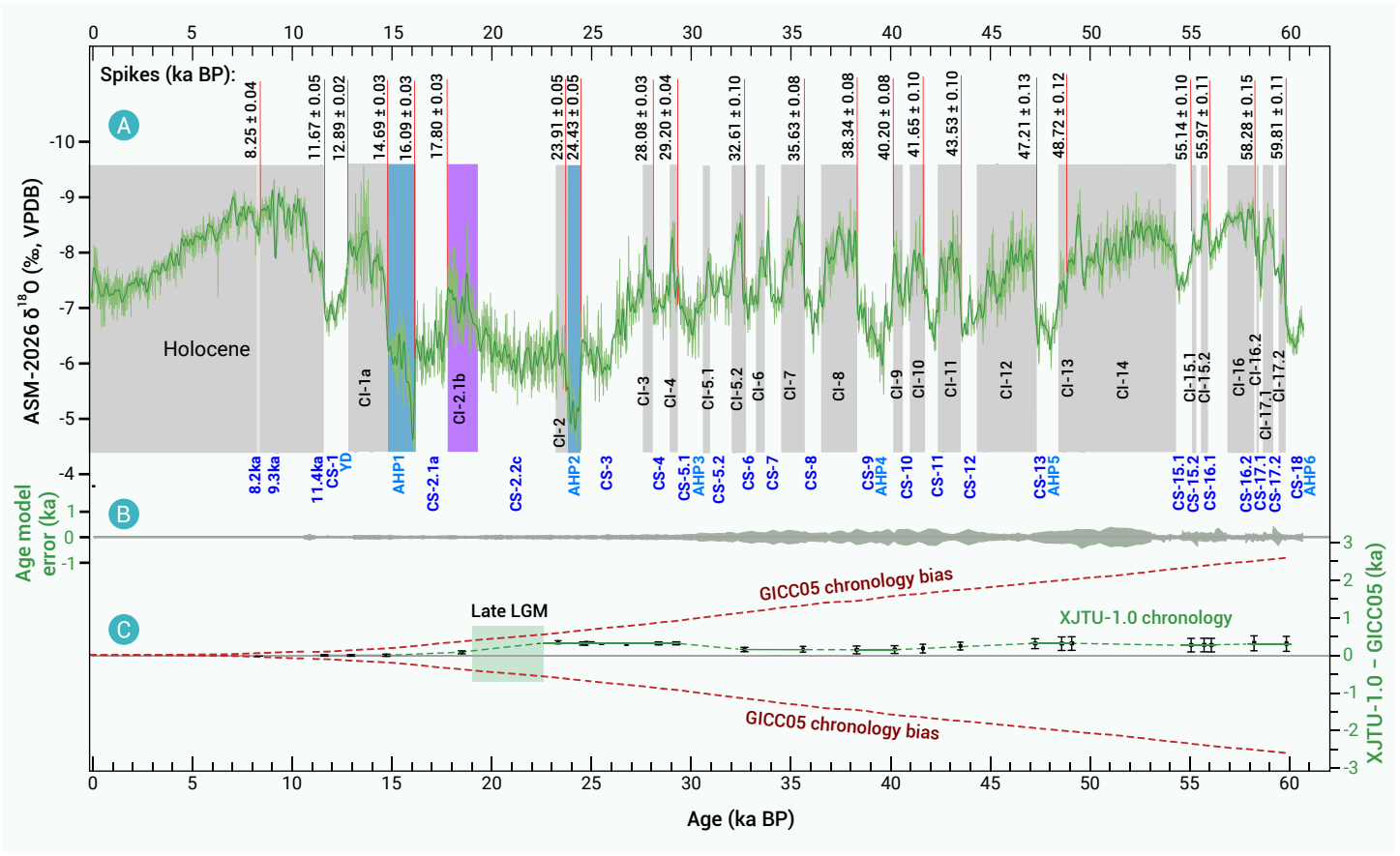

Figure 1. Speleothem-based XJTU-1.0 geochronology and uncertainties (A) The ASM-2026 $\delta^{18}O$ record (light green) and the 10-point smoothed curve (green, this study). The dates at the top show the age of important spikes (refs.[7,9,15,16,29,32] and this study). Note that the age spikes at CI-10 and CI-11 are from ref.[48]. The 8.2 ka event, YD, CSs-CIs, and AHP are labeled. (B) Age model uncertainty of the XJTU-1.0 chronology. (C) Chronological difference between XJTU-1.0 (this study) and GICC05.[2] The error bars indicate the speleothem-based age spikes and their differences from GICC05. Two red dashed lines show the age error estimate for GICC05.[2] The largest offset (~320 years) occurs around the late last glacial maximum (LGM) as indicated by the transparent green box.[7]

cal spikes used for this period come from several other cave speleothem records from the ASM domain (refs.[15,16,29,44] and this study). As detailed in Table S1, this study first employed the Bayesian ensemble algorithm (BEAST)[46] to derive breakpoint ages for the MSD record and identified the corresponding sampling depths. Subsequently, we recalculated the MSD record's OxCal age model to reconcile the breakpoint ages of the MSD record with the target chronological spikes (Table S1).

Collectively, the chronology of the ASM-2026 record, XJTU-1.0, represents the state-of-the-art in the research forefront, which provides a set of chronological benchmarks for correlating and calibrating climate variabilities over the past 60 ka (Figures 1 & S4). In essence, each chronological benchmark in XJTU-1.0 relies largely on the precise timing of the abrupt monsoon transition constrained by a large number of U-Th dates. While the XJTU-1.0 is robust within uncertainties, a caution is still warranted when interpreting the $\delta^{18}O$ amplitude variation. This is because the ASM-2026 record integrates speleothem datasets from multiple caves (Table 1), and each of them might be influenced by site-specific hydrological and epikarst effects. Nevertheless, the main part of ASM-2026 consists of records from Hulu and Dongge caves that are broadly comparable regarding their variabilities.[33,47] As such, the monsoon variability, including relative amplitudes, appears to be reliable, such as larger amplitudes for events associated with HSs compared with those associated with ordinary DO events. For small-amplitude comparisons involving cave records other than those from Hulu and Dongge caves, we recommend applying site-specific corrections to account for possible inter-cave isotopic offsets.

RESULTS AND DISCUSSION

Speleothem-based geochronology and correlation strategy

U-Th dated speleothem $\delta^{18}O$ records from the ASM domain have been previously used to provide precise chronological benchmarks for correlating and calibrating climate variability on centennial to orbital scales (e.g., refs.[16,27,29,31,33,45,49,50]). However, the timing of some abrupt ASM events during the last glacial period appears to differ considerably among cave $\delta^{18}O$ records.[51-52] To tackle the issue, we conducted extensive high-precision dating of distinct abrupt climate events (e.g., the 8.2 ka event, the YD and HSs1–4) in cave $\delta^{18}O$ records from the ASM domain. These studies have clearly demonstrated that significant abrupt climate events recorded by different ASM cave records occurred synchronously within dating uncertainties (e.g., refs.[7,9,15,16,29,31,32]). This has also led to the development of precise chronological benchmarks for abrupt climate events such as the 8.2 ka event,[8] the YD,[9] Asian Heinrich Period (AHP) 1 (corresponding to HS1),[32] AHP2,[7] AHP3,[29] AHP4,[15] and Chinese Interstadial (CI, corresponding to GI) 15.1,[16] etc. We further established causally sound correlation strategies between the ASM cave $\delta^{18}O$ record and a number of other key climate records across HSs and other events in various climate systems worldwide[7,9,14-16,29,31-33,53] (Text S1), including the Greenland ice-core $\delta^{18}O$ records, atmospheric CH_4 records from Antarctic ice cores (and in turn gas records of CO_2 and $\delta^{18}O$ of O_2), Antarctic ice $\delta^{18}O$ and other proxy records in the ice phase through bipolar volcanic spikes,[28] and the North Atlantic sea-surface temperature (SST) and correlated changes in AMOC, IRD, and benthic $\delta^{18}O$ through Greenland $\delta^{18}O$ records.[54]

In this study, we developed a new high-resolution (~8 years) composite cave $\delta^{18}O$ record (ASM-2026, Data S2), derived mainly by combining previous and new high-resolution Hulu cave $\delta^{18}O$ data (this study) from ~53.06 to 19.26 ka BP, and by incorporating several short-duration datasets from other cave $\delta^{18}O$ records (Wulu, Shennong and Dongge caves) (Figure S2 & Table 1; MATERIALS AND METHODS). ASM-2026 was first anchored to a set of selected high-precise chronological benchmarks previously determined over the past 60 ka, and then we further established precise time series for additional abrupt ASM events, i.e., CS-13 (AHP5), CS-15.1 (AHP5a), and CS-18

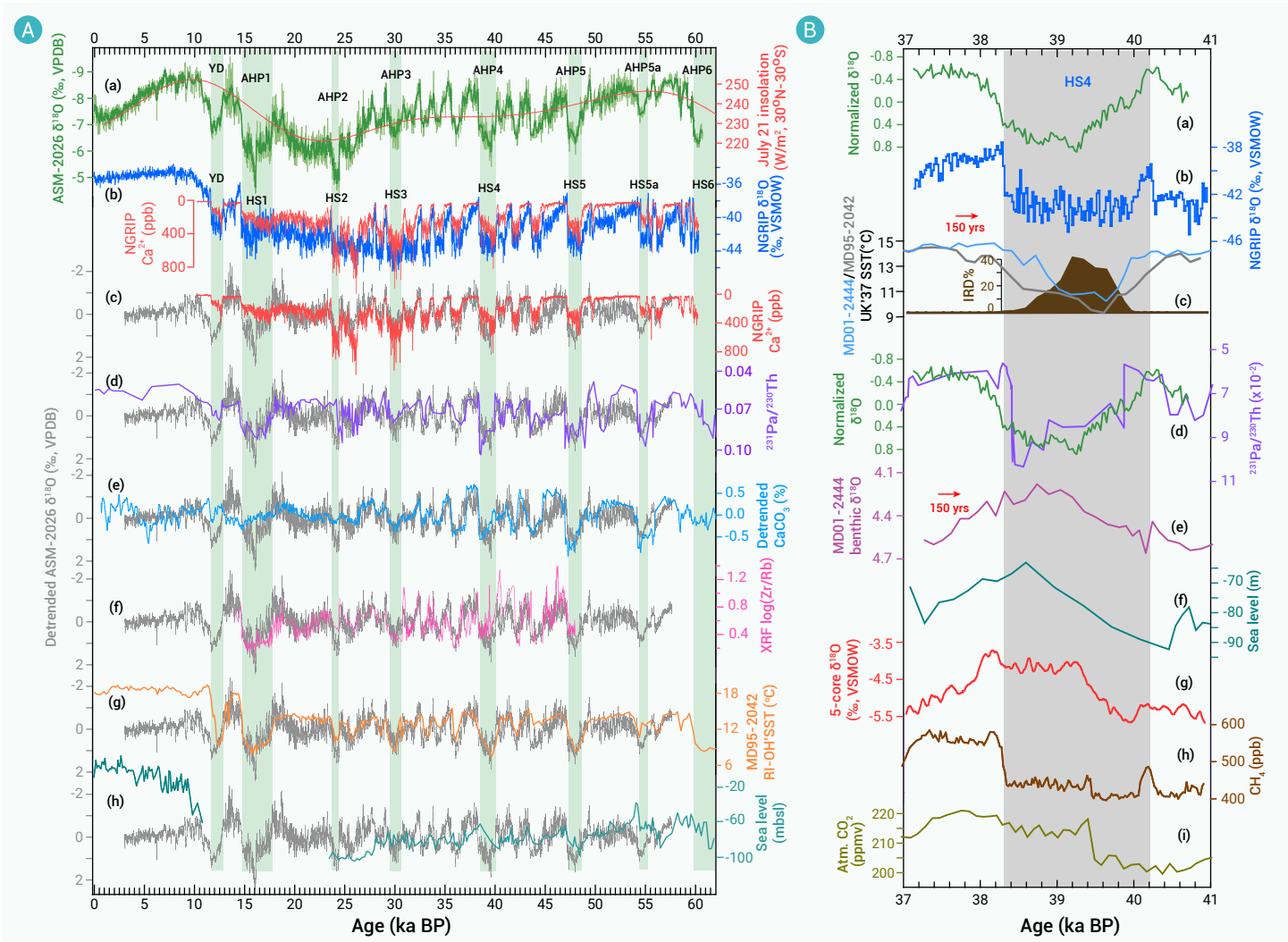

Figure 2. Relation between ice volume and ASM on millennial-scales (A) for the last 60 ka: (a) ASM-2026 record (green, this study) and July 21 insolation difference between 30°N and 30°S[60] (red). (b) Greenland NGRIP $\delta^{18}O$ (blue) and Ca^{2+} (red) records[2,61] on the XJTU-1.0 chronology. (c) Greenland NGRIP Ca^{2+} (red) record[22] on the XJTU-1.0 chronology. (d)–(e) Bermuda Rise $^{231}Pa/^{230}Th$[62,63] (purple) and CDH19 core $CaCO_3$ (%)[63] (blue) records, both indicating AMOC strength. (f) Composite XRF log (Zr/Rb) record from the North Atlantic (pink), a qualitative indicator of near-bottom current flow speed indicating the AMOC strength.[64] (g) North Atlantic SST proxy record (orange).[65] (h) Sea level relative to present day (jade).[66] Grey curves in (c)–(h) show the detrended ASM-2026 record (after removing the insolation component, this study). (B) for the HS4: (a) Composite $\delta^{18}O$ record from the four ASM domain cave records.[15] (b) Greenland NGRIP ice-core $\delta^{18}O$ records[2] on the GICC05 chronology[57] with a shift of +150 years[15] to match the XJTU-1.0 chronology. (c) Reconstructed sea-surface temperature (SST) from North Atlantic MD01-2444[67] (blue) and MD95-2042 cores[65] (grey), and ice-rafted debris percentage from MD01-2444 core[67]. (d) Composite cave $\delta^{18}O$ record from the four records[15] (green) and Bermuda Rise $^{231}Pa/^{230}Th$ record[63] (purple). (e) Benthic $\delta^{18}O$ record from MD01-2044 core.[67] Note that marine sediment records in (c) and (e) have already been tuned to the GICC05 chronology,[53] and thus been further shifted by +150 years.[15] (f) Sea level relative to present day.[66] (g) Antarctic 5-core averaged $\delta^{18}O$ record.[49] (h) Antarctic WDC ice-core CH_4 record.[68] (i) Antarctic WDC ice-core CO_2 record.[69] Proxy records in (g)–(i) are plotted on a chronology synchronized with the XJTU-1.0 chronology (MATERIALS AND METHODS).

(AHP6) (Figure S5 & Text S2), leading to a much more precise chronology for ASM-2026, XJTU-1.0 (Figure 1 & Data S2). The absolute age uncertainties (2σ) of XJTU-1.0 increase gradually over the past 60 ka from the younger (~40 years) to the older (< 500 years) portions, considerably more precise compared to the Greenland Ice Core Chronology 2005 (the GICC05 chronology)[55-58] with reported age uncertainty from ~200 years at the YD to ~2600 years at HS6 (the maximum counting errors) (Figure 1).[2] ASM-2026 on the XJTU-1.0 chronology not only offers a precise frame to characterize ASM variability over the last 60 ka, but also allows a more realistic correlation and calibration of key global hydroclimate variabilities (Text S1 & Figure S6). This, in turn, provides a crucial basis for further addressing a number of outstanding issues in the forefront of the field.

The ice volume and ASM dynamics

Variations in the global ice volume (or northern high-latitude ice sheets) have long been hypothesized as an important driver of ASM variability in such that a large global ice volume (or NH ice sheets) suppresses ASM and vice versa (e.g., ref.[59]). However, while a number of recent studies show that the insolation forcing prevails in driving orbital-scale ASM dynamic variability (e.g., refs.[26,40]), the influence of the ice volume forcing on the ASM needs further scrutiny at millennial-scale. In this regard, advances in the correlation framework and synchronizations of marine, ice core, and cave records over the past 60 ka (Figures 2, S4 & S6) allow us to decipher whether the ice volume change was a significant driving force behind ASM dynamics. The last deglaciation (~19 to 8 ka BP) was a period marked by ice sheet melting (or global sea level rising and the ice volume waning) associated with an increasing global surface temperatures and atmospheric CO_2 concentrations. Superimposed on this trend was a sequence of millennial-scale and quasi-stable climate intervals documented by numerous climate archives, specifically the cold HS1 (~17.5–14.70 ka BP, including HE1), the Bølling-Allerød (BA) warm period (~14.70–12.87 ka BP), the cold YD (12.87–11.70 ka BP) and the warm Holocene (since ~11.70 ka BP) (Figures 1 & 2A). Apparently, the millennial-scale ASM sequence superimposed on the last deglaciation is comparable to the large abrupt changes in their North Atlantic counterparts, namely CS-2.1a (GI-2.1a) and AHP1 (HS1), CI-1 (BA), CS-1 (YD) and the abrupt onset of the Holocene (Figure 1), while the ice volume was characterized by a persistent and gradually decreasing trend from ~19 to 11 ka BP (Figures 2A & S4). This indicates that the ice volume forcing may have a

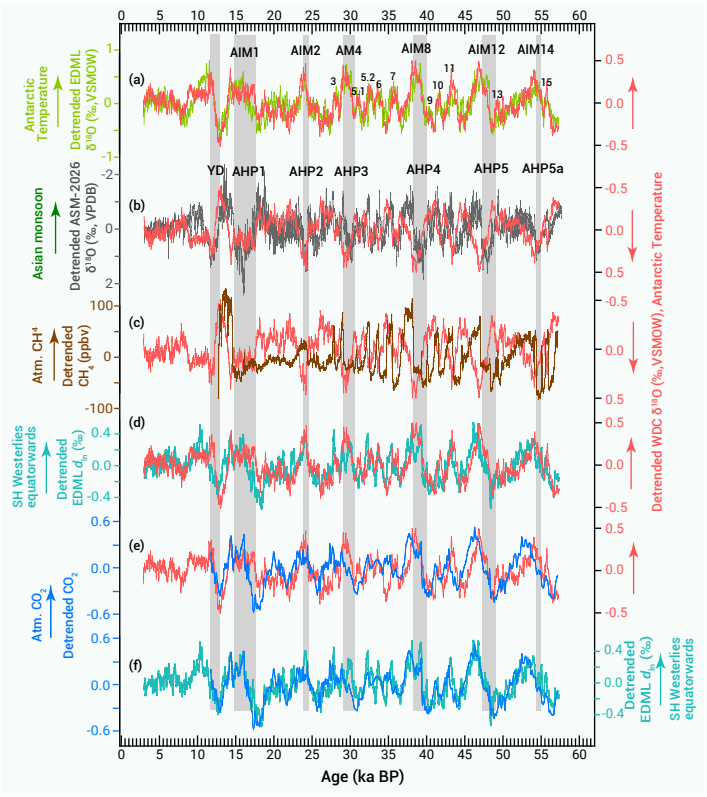

Figure 3. Comparison between detrended Asian monsoon, Greenland and Antarctic ice-core records for the last 60 ka (a) Detrended Antarctic EDML $\delta^{18}O$ record (yellow-green).[24] (b) Detrended ASM-2026 record (grey, this study). (c) Detrended Antarctic ice-core WDC CH_4 record (brown).[68] (d) Detrended Antarctic EDML d_{ln} (teal) record.[24] (e) Detrended composite atmospheric CO_2 record (light blue).[69] Red curves in (a)-(e) are the detrended WDC $\delta^{18}O$ record.[24] (f) Detrended Antarctic EDML d_{ln} (teal)[24] and detrended composite atmospheric CO_2 record (light blue).[69] Grey bars show AHPs.

negligible impact on ASM dynamics on millennial-scales (Figures 2 & S7-S8). For example, (1) while the ice volume decreased during the AHP-1 and YD, the ASM remained in a pronounced weak state; and (2) while the ice volume was nearly at its maximum around 18–19 ka BP, the ASM reached an apparent peak that coincided broadly with a strong AMOC state (Figure S7).

To date, the role of the ice volume during millennial-scale events, such as HSs, remains understudied partially due to the low resolution and a lack of precise chronology in marine records, as well as uncertainties in the interpretation of the benthic $\delta^{18}O$ records (ice-volume change versus deep ocean temperature change). Nevertheless, it appears that a decrease (increase) in benthic $\delta^{18}O$ occurred during prominent GSs (GIs) (such as HS4 and subsequent GI-8) (e.g., refs.[17,21,70-72]) (Figure S7), and, if assuming benthic $\delta^{18}O$ could reflect ice volume changes to some extent, then the ice volume would apparently decrease during HS4 (increase during GI-8), corresponding to waning (waxing) state of the ASM (Figures 2 & S7). This correlation is robust because the North Atlantic benthic $\delta^{18}O$ records can be linked to the Greenland ice-core chronology via their SST (or IRD) and/or sediment $^{231}Pa/^{230}Th$ records on the same timescale (Figure S7).[14,53,73] A similar relationship becomes even clearer during the penultimate termination process (AHP11/HS11),[14,31] lending a support to our interpretation since millennial-scale events are essentially the 'low-amplitude version of terminations' (Figure 2B).[74] On the other hand, millennial-scale climate variations deciphered from ASM cave records manifest a considerable similarity to change rates in the ice volume, suggesting that the melting rate of the ice sheet, rather than the ice sheet itself, plays a critical role in driving the ASM, apparently through changes in the North Atlantic fresh water forcing, which changes the AMOC mode and in turn the ASM dynamics.[34]

Another outstanding issue lies in the notion that the ASM millennial variability may be dominantly controlled by SH climate changes during the last glacial (e.g., refs.[75,76]), suggesting a so-called 'push' forcing on the boreal ASM originating from cooling of the SH. This forcing was hypothesized to link dynamically to the equatorward temperature gradient increase in the SH inferred from Antarctic temperature records, which leads to an intensified cross-equatorial airflow, and thus the boreal ASM circulation.[76,77] Broadly, millennial variabilities in Antarctic ice-core temperature, δD, $\delta^{18}O$, CO_2, and d_{ln} records are characterized by more gradual 'Antarctic-type' changes, in contrast to more abrupt 'NGRIP-type' changes (e.g., recorded by Greenland $\delta^{18}O$ and Ca^{2+}) (Figures 3 & S4). On the other hand, high-resolution and precisely dated ASM $\delta^{18}O$ records also show that ASM transitions, in response to AMOC changes, are considerably more gradual compared to the NGRIP $\delta^{18}O$ record (e.g.,[15,29,32,78]). However, over the past decade, precise synchronizations of Greenland and Antarctic ice-core records during the last glacial period have clearly shown that abrupt climate changes in Greenland lead Antarctic responses by ~200 ±100 years[27] and subsequently revised to ~60 years.[79] Since millennial-scale ASM events correspond to Greenland abrupt changes regarding their onset,[7,9,15,16,29] the ASM strengthening (weakening) should lead to, rather than lag behind, Antarctic cooling (warming) inferred from Antarctic ice core $\delta^{18}O$/δD (mainly temperature proxies) records.

Essentially, up until now, the phases between the ASM and Antarctic temperatures are not well constrained on the millennial scale, because age uncertainties from both ASM and Antarctic records (hundreds of years) preclude such a precise synchronization. In the XJTU-1.0-based correlation framework (Figures S4 & S6; MATERIALS AND METHODS), the ASM intensification leads the Antarctic cooling (negative excursions of the $\delta^{18}O$ and δD) by ~0.88, 0.65 and 0.36 ka highlighted at the millennial-scale coherent bands centered at ~4.5, 2.8 and 1.5 ka, respectively (Figure 4). The uncertainty of the phase lead in the last glacial period comes mostly from the correlation between ASM and Greenland $\delta^{18}O$ as well as the bipolar volcanic matching. The former uncertainty is in sub-centennial to centennial ranges for a large portion of the last glacial (e.g.,[7,9,15,16,29]) (Figures 1 & S4), and the latter is estimated to be precise at decadal-scale.[28] Both, or their combined uncertainties, are generally smaller than the estimated ASM phase-lead relative to the Antarctic temperature (Figure 4). This implies that the SH 'push' may not be the primary driver of the ASM millennial variability during the last glacial, specifically at the ~4.5-ka frequent band. Moreover, on glacial-interglacial scales, Antarctic gradual cooling[27] and the increase of the simulated total Antarctic ice volume[80] correspond to the ASM weakening (rather than strengthening) from ~60 to 22 ka BP (Figure S4). In West Antarctica, warming began at ~22 ka BP and continued until ~8 ka BP, while in East Antarctica it started later at ~18 ka BP; overall, this Antarctic warming corresponds to an overall ASM strengthening (rather than weakening) during these intervals (Figure S4). These results do not appear to support the notion that the ASM strengthens drastically in response to an increased cross-equatorial pressure gradient forced by SH high-latitude cooling on glacial-interglacial scales.[77] Further model simulations are needed to pinpoint the underlying dynamics, and our observations, refined using the synchronized chronology, provide vital constraints on the relationship between the ASM and SH hydroclimate.

Additionally, in the Antarctic ice core records, millennial variabilities in $\delta^{18}O$, d_{ln} and CO_2 records (Figures 4 & S9) show coherent bands centered at ~8 and 4.5 ka. The CO_2 variations have long been considered to track Antarctic changes or to be controlled largely by SH processes. In our phase analyses, CO_2 appears to lag Antarctic temperature (inferred from $\delta^{18}O$) by about 1.1 and 0.35 ka on millennial bands centered at ~8 and 4.5 ka (Figure S9D), which is consistent with the observation that peak CO_2 levels lag peak Antarctic temperatures by more than 0.5 ka.[69] Intriguingly, CO_2 is highly correlated with the Antarctic precipitation d_{ln} (r =0.72 [0.70, 0.73], 95% confidence interval) with virtually the same phase (~200-year difference, but within the margin of uncertainty) (Figures 4 & S9C). Currently, the leading hypothesis about the CO_2 rise during the last glacial involves stronger SH westerly winds, especially their stress and poleward shift, which boost CO_2 outgassing from the Southern Ocean via increasing the upward transport of dissolved inorganic carbon in the Circumpolar Deep Water, leading to atmospheric CO_2 increase.[81,82] The Antarctic d_{ln} reflects mainly the weighted mean evaporative conditions over the oceanic moisture source regions, whose spatial distribution is sensitive to changes in the atmospheric circulation, involving the stress and position of the SH Westerlies,[83] as well as the South-

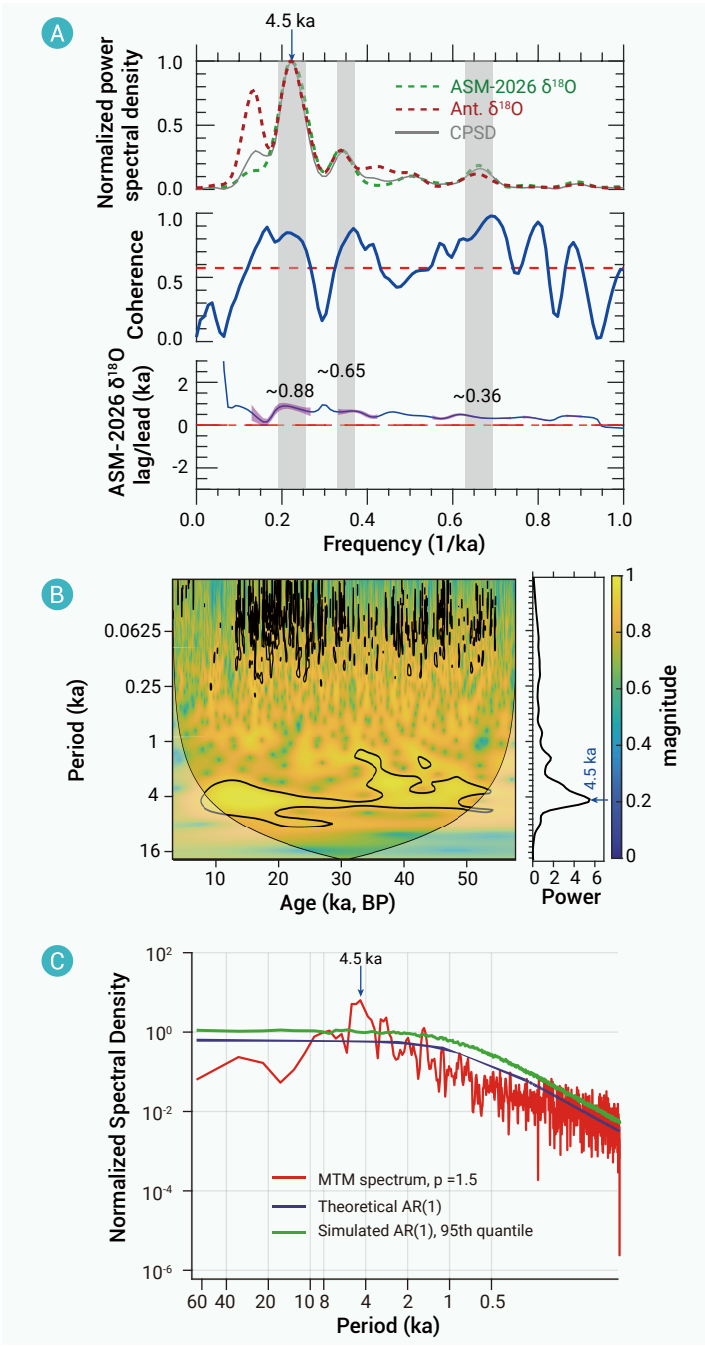

Figure 4. Spectral and wavelet analyses of millennial-scale variations (A) Cross spectrum analysis. Top: Normalized spectral density of the ASM-2026 $\delta^{18}O$ (green dashed line), Antarctic ice-core $\delta^{18}O$ (red dashed line) and cross power spectral density (CPSD, grey solid line) between ASM and Antarctic ice-core $\delta^{18}O$. Middle: Coherence spectra marked by grey bars. Bottom: Phase relation. ASM $\delta^{18}O$ leads Antarctic ice-core $\delta^{18}O$ variations by ~0.88, ~0.65 and ~0.36 ka as highlighted by grey bars at millennial bands centered at 4.5 ka, 2.8 ka and 1.5 ka, respectively. The horizontal dashed line in the middle panel marks the significance limit corresponding to the 0.58 threshold (80% confidence interval). In the bottom panel, the purple shading denotes the 80% confidence interval for the phase errors. (B) Wavelet analysis result for the detrended ASM-2026. Black contour indicates the 95% significance level relative to the red noise. (C) Multitaper power spectral density estimated for millennial variations of the detrended ASM-2026 over the last ~60 ka. The term p is the time-bandwidth product. Purple line shows the theoretical power spectrum of a first-order autoregression model (AR1). Green line shows the 90% confidence interval of a 500-ensemble Monte Carlo test. The most prominent millennial cycles of ~4.5-ka are shown by blue arrows (A)–(C).

ern Annular Mode.[24] This causal nexus may primarily explain the observed correlation between Antarctic d_{ln} and CO_2.

Dominant pattern of the millennial variability

As shown by a large number of empirical and modeling studies, the insolation forcing, rather than the ice volume, plays a key role in driving the ASM dynamic variability on orbital-scales.[33,34] On millennial-scales, empirical records reveal a close relationship between the AMOC and the ASM, not only during the deglaciations (Figure S7),[31] but also throughout the last glacial period (Figure 2). This is clearly demonstrated by an apparent covariance between ASM and AMOC proxy records, such as $^{231}Pa/^{230}Th$ records from the Bermuda Rise,[62,63] XRF log (Zr/Rb) records from the North Atlantic,[64] and $CaCO_3$ (%) records from CDH19 core in the North Atlantic (Figure 2A).[63] Mechanistically, this is because the ASM is largely driven by AMOC, and thus behaves as one of cascading results of AMOC changes (e.g., refs.[29,34]). This has been demonstrated persistently through a series of model studies (e.g., refs.[29,84]). Of note is a high-degree similarity of AMOC reconstructions with a set of important climate records that are largely influenced by the AMOC, such as ASM-2026, North Atlantic SST, temperature of the European Alps, etc. All of these records are characterized by a more 'quasi-trapezoidal' pattern of DO cycles, which is distinct from the typical 'sawtooth' pattern of Greenland ice-core $\delta^{18}O$ records (Figures 2A & S10-S11). Actually, the Greenland ice core Ca^{2+} (or dust) record, mainly a proxy of the strength and position of the Asian Westerlies,[7,85] also exhibits a quasi-trapezoidal pattern more similar to ASM-2026, but substantially different from the sawtooth pattern in the corresponding Greenland ice-core $\delta^{18}O$ records (Figures S10-S11). As such, a quasi-trapezoidal pattern, rather than a sawtooth pattern represented by Greenland precipitation $\delta^{18}O$,[29] may be the dominant climate oscillation pattern, which is more appropriate as a reference for climate research at millennial-scales.

Another critical observation is that major climate records, such as ASM, AMOC, North Atlantic SST, and Indian/East Asian/South American monsoon records, show more pronounced amplitudes during HSs than during non-Heinrich stadials, in contrast to the Greenland ice-core $\delta^{18}O$ records (e.g., refs.[7,29,65]) (Figure S11). Particularly, variations of millennial ASM events align closely with changes in AMOC strength (e.g., ref.[63]) with markedly weakened AMOC and ASM during HSs/AHPs compared to non-Heinrich stadials (Figure 2A). In contrast, Greenland ice-core $\delta^{18}O$ may be more complicated due to multiple effects besides the Greenland local temperature, such as moisture source change (or sea-ice dynamics),[29] or precipitation seasonality.[86] Consistently, model studies have clearly demonstrated a coupling between ASM and AMOC.[84,87] As such, our ASM-2026 record may tentatively serve as an alternative to existing AMOC time series, which has high-resolution and precise age control compared with present AMOC proxies from the North Atlantic (Figures 2A & S10). Since ASM-2026 presumably reflects cascading responses/feedbacks causally linked closely to AMOC, and in that regard it indicates the 'effective AMOC intensity' compared to the current North Atlantic proxies of the AMOC that may be subject to various uncertainties, such as the injection points of meltwaters and ocean circulation conditions.[88,89]

Millennial climate cycles

Over the past four decades, extensive research has focused on millennial-scale climate oscillations throughout the past 800 ka, but whether their rhythms were driven by periodic forcings or occur stochastically remains uncertain. A number of studies show diverse periodicities in millennial climate oscillations, such as ~1.5-ka,[90] ~2.4–2.8-ka,[91] ~4-ka,[92] ~4.5–5.5-ka[93-95] and ~6–7-ka.[96] However, it is still unclear whether a dominant period persists globally, and if so, whether the underlying mechanism is related to internal climate processes or external orbital-driven changes in insolation, or both.[97] This hinders our understanding of the cause of millennial oscillation. Our analyses of the detrended ASM-2026 (Text S3) reveal the most prominent millennial cycles of the ASM at ~4.5-ka over the last 60 ka (Figure 4). In fact, this cycle is also the most prominent millennial cycle of the ASM over the past 690 ka (Figure S12A). Similar cycles are also revealed in other thermodynamic records of the Asian monsoon, such as loess Fe/K record (precipitation) from Chinese Loess Plateau and the AP% record (temperature) from the Zoige Basin.[98] Furthermore, the ~4.5-ka cycle does not appear to be confined to the ASM domain, rather, it has a global scope, as it also dominates in Greenland NGRIP $\delta^{18}O$ (primarily a temperature proxy, over the last ~120 ka), Antarctic $\delta^{18}O$ and δD (primarily Antarctic temperature proxies), and atmo-

spheric oxygen $\delta^{18}O$, CO_2 and CH_4 records (over the last 800 ka) (Figures S9 & S12-S13). Particularly, the in-phase results from spectral analyses for high-resolution NGRIP ($\delta^{18}O$ and Ca^{2+}) and ASM-2026 are robust (Figures 4, S9 & S12-S13), because their chronologies have far smaller uncertainties for such analyses (Figure 1). In sum, the ~4.5-ka cycle appears to be the most prominent millennial cycle over the past 800 ka, a typical icehouse interval in the Earth's history, but whether it represents an independent forcing or derives from higher-frequency oscillations (e.g., ~1.5-ka) remains to be explored.

A recent study revealed that the most prominent millennial climate cycle was ~4.5-ka in the early Late Cretaceous, a typical greenhouse period in the Earth's history.[99] This cycle, corresponding to one-quarter of the precession cycle, is attributed to a precession-stimulated millennial climate cycle or an equatorial insolation mechanism. Theoretically, the climate response to the largest amplitude of the seasonal cycle of equatorial insolation induced by precession could instigate the millennial climate cycle at ~5-ka (i.e., ¼ precession).[100] The high-quality reconstruction of the millennial dry-wet oscillation in the early Late Cretaceous[99] is in excellent agreement with the theoretically-predicted equatorial insolation[100] in terms of both the periodicity and intermodulation structure. This analysis leads to a supposition that the persistent ~4.5-ka cycle inferred from the geological archives in the early Late Cretaceous was triggered by an equatorial insolation mechanism.[99] In other words, the most prominent ~4.5-ka climate cycle observed under greenhouse conditions can be attributed to the forcing of the equatorial insolation that was theoretically predicted. A subsequent question is whether this same equatorial insolation forcing can explain the ~4.5-ka climate cycles that have recognized over the past 800 ka under icehouse conditions. In principle, the theoretical insolation forcing should also influence the climate system under icehouse conditions; however, it can be expected that the way this forcing acted may differ to some extent over the past 800 ka, because an icehouse is essentially different from a greenhouse, particularly regarding land-sea distribution, ocean/atmosphere circulation, polar ice sheets, and atmospheric CO_2 levels. For example, dynamics of AMOC and NH ice sheets play an important role in promoting millennial climate cycles during icehouse periods.[10] However, these icehouse-specific dynamics are presumably absent in the greenhouse conditions. Given the fact that the oscillatory modes within the Earth's climate system are far more sporadic in terms of periodicity, especially across greenhouse and icehouse conditions, one of plausible hypotheses is thus that the 'clock' triggering the ~4.5-ka climate cycle resides outside the Earth system, making the equatorial insolation forcing one of most plausible candidates. A further examination also found that the ~4.5-ka component in the ASM cave $\delta^{18}O$ record over the past 690 ka is significantly modulated by 100-ka and 405-ka eccentricity cycles, suggesting that it likely originates from precession-related equatorial insolation (Figure S14). If this is the case, then low-latitude regions, which receive the most external solar radiation, may play a more significant role in triggering millennial climate cycles than previously assumed. Over the past decade, model simulations indeed show that orbital precession thresholds and peaks can lead to AMOC variations,[64,65] lending credibility to the insolation mechanism(s). Nevertheless, a major gap remains in understanding the linkage between the equatorial insolation forcing and the AMOC dynamics underlying millennial climate variability, which is still a mystery that urgently requires further investigation through both empirical and modeling studies.

Termination of Heinrich stadials

It has long been recognized that HSs manifest pluvial periods in South America (e.g., refs.[17,21]) (Figure S15), which may provide critical positive feedback that sustains a weakened AMOC via the freshwater forcing of the Amazon River discharge.[15] On the other hand, recent studies also indicate that the termination of major millennial-scale events such as HS4 and HS2[7,15,34] is preceded by a multi-centennial drying trend across the vast SAM domain, and thus a reduced Amazon River discharge into the tropical Atlantic Ocean (Figure S16). Our new data also indicate that terminations of HS3 and HS5 were associated with centennial-scale earlier terminations of the SAM (or pluvial periods) (Figure S17). This suggests that at least the terminations of HSs likely began with a centennial-scale weakening of the SAM, preceding the corresponding terminations of Greenland HSs, thereby indicating a more active role of low-latitude hydroclimate changes (Figure 5). On the other hand, numerous marine sediment records of river discharges (such as Ti/Ca, Ba/Ca, and Fe/Ca) also indicate substantially higher fluvial discharges in northeastern Brazil during HSs (e.g., refs.[101-106]), which presumably correlate to SAM rainfall amounts, and in turn the SAM cave $\delta^{18}O$ negative excursions during HSs (Figures S15-S16). Although precisely estimating increases in fluvial discharge is challenging, significantly higher Ti/Ca (and Fe/Ca) ratios during HSs suggest that fluvial discharge far exceeded the modern value of 0.18 Sverdrup (Sv). For instance, Ti/Ca ratios surge dramatically from virtually zero to ~0.8 during HSs (Figure 5). Noticeably, the significant increases in fluvial discharge occurred along a very large portion of the western Atlantic trajectories of the surface 'great conveyer belt' (i.e., the AMOC surface branch), including both the North Brazil Current and the North Brazil Undercurrent (Figure S16). Therefore, the South American large fluvial input during HSs and its earlier termination acted as a freshwater forcing, which may have played a profound role in maintaining the HS mode of the AMOC and stimulating the subsequent reinvigoration—a hypothesis outlined earlier in refs.[15,34].

The triggering mechanism of earlier terminations of the South American pluvial periods (corresponding to HSs) remains unclear.[7,15,34] Modern climatology shows that both the Antarctic Oscillation (AAO) and El Niño/Southern Oscillation (ENSO) significantly influence the spatial pattern of rainfall over South America (Figure S18). The AAO, also referred to as the Southern Annular Mode, is the dominant pattern of circulation anomaly variability in the SH.[107] It is defined as a belt of strong mid-latitude westerly winds (~40°S) or low-pressure surrounding Antarctica (~65°S)[108] with the SH Westerlies displaced equatorward at the AAO− phase and vice versa. From AAO+ to AAO−, overall rainfall decreases (increases) in northern (southern) South America significantly, resulting in drier condition in the Amazon River Basin and surrounding regions (Figure S18). On the other hand, the isotopic compositions ($\delta^{18}O$ and d_{ln}) of Antarctic ice cores can be theoretically and empirically linked to Southern Ocean SST variations. Warming in both Antarctica and the Southern Ocean vapor source regions corresponds to a poleward intensification of the SH Westerlies, indicating an AAO+ like mode, and vice versa.[25,108] A detailed examination of $\delta^{18}O$ and d_{ln} from Antarctic ice cores—especially the EDML ice core from the Atlantic sector—revealed a shift from an AAO+ like mode to an AAO− like mode prior to terminations of HSs. This shift is inferred from the decreasing trends in d_{ln} (Figure S19), which lasted hundreds of years, comparable to the durations of the early termination of South American Heinrich Periods (SAHPs).[7,15,34] The transition of the AAO mode from a positive to a negative phase may result in drought conditions in northern South America and pluvial conditions in southern South America. Consequently, this would diminish the freshwater discharge from the Amazon River and other rivers in northeastern Brazil (Figures S16 & S18). Moreover, modern climate data reveal a significant negative correlation between ENSO and AAO (Figure S18A). If this relationship holds true for HSs, the observed shift from an AAO+ like mode to an AAO− like mode would coincide with a transition from a more La Niña-like state to a more El Niño-like state. This change would reinforce drought conditions in northern South America and pluvial conditions in southern South America toward the end of HSs (Figure S18). This preliminary mechanism provides a new conceptual understanding, highlighting the active role of low-latitude and SH climate dynamics in driving millennial-scale climate variations.

Multidecadal-centennial variability

Analyses of the NGRIP $\delta^{18}O$ record in both temporal and frequency domains reveal an interesting pattern that the Holocene is marked by lower-amplitude (< 1‰) and shorter-periodicity (~30-years) variability in contrast to the larger variability (~2‰) and periodicity (1000–60 years) seen during the glacial period (Figures 6B & S20B). However, it has been suggested that the lower-amplitude variability during the Holocene may partly result from the diffusion of water vapor within the firn, which can attenuate the original isotopic signals because of enhanced smoothing at higher temperatures (e.g., ref.[109]). In contrast, the speleothem $\delta^{18}O$ records are generally unaffected by such a diffusion process or post-formation changes. Yet, detecting robust spectral power from speleothem $\delta^{18}O$ records has been limited by the lack of rigorous age control and the progressive increase in age uncertainty with time. ASM-2026 is primarily based on the Hulu and Dongge cave records (~53 ka BP to present) that are comparable in terms of their $\delta^{18}O$

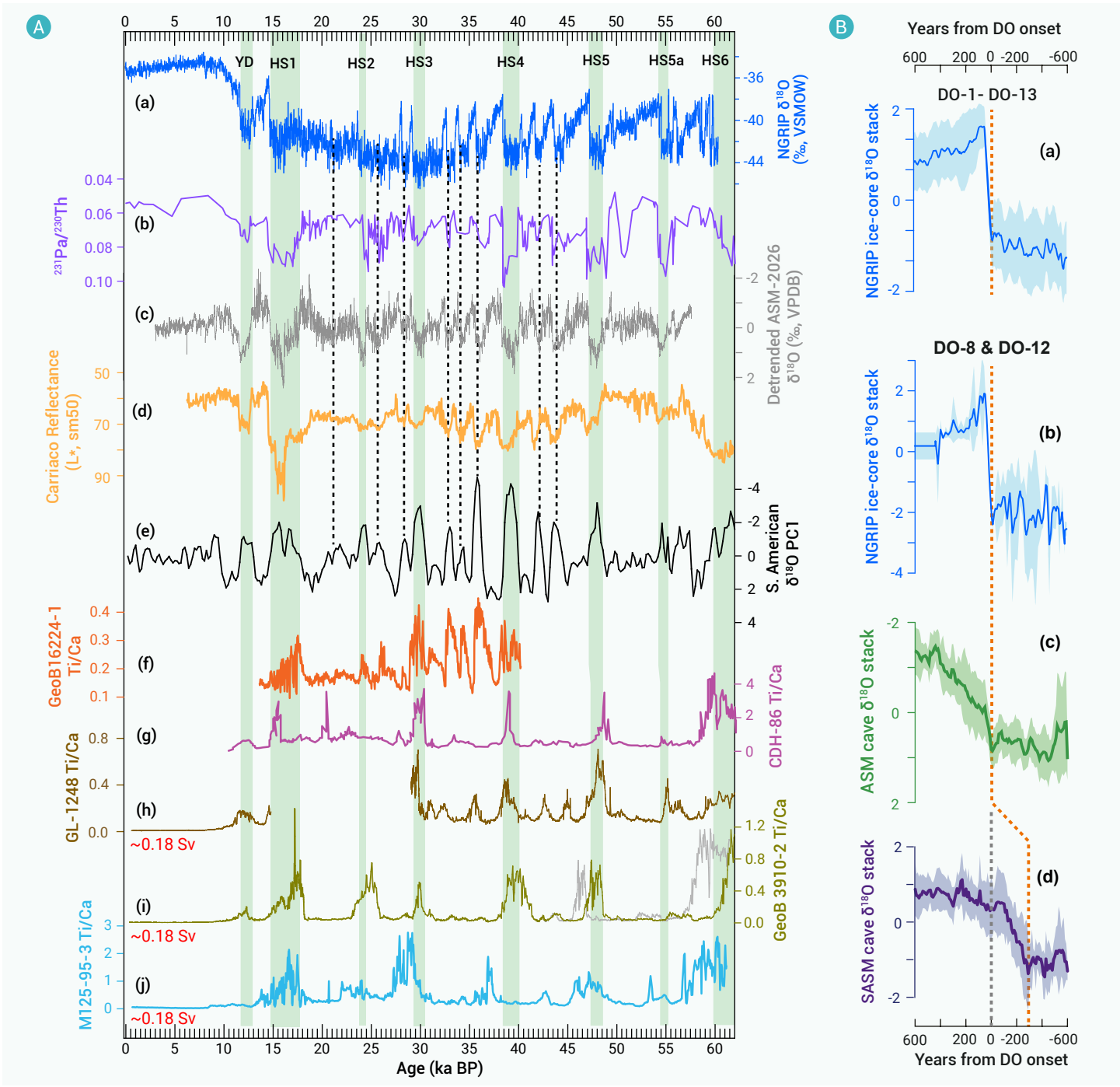

Figure 5. Climate variability across the last 60 ka (A) Comparison between ice core, marine sediment, ASM and SASM records. (a) NGRIP $\delta^{18}O$ records[2,61] (adjusted to XJTU-1.0 chronology). (b) Bermuda Rise $^{231}Pa/^{230}Th$ records (AMOC strength proxy).[62,63] (c) Detrended ASM-2026 (this study). (d) Lightness (L*) from northern South American core MD03-2621[12] (500-year lowpass-filtered after 50-year interpolation). (e) Composite SAM cave $\delta^{18}O$ records from East Amazon, West Amazon, central Brazil and Southeast Brazil (see Text S4, Table S2, Figure S15 & Data S3). (f)-(j) Ti/Ca record from marine sediment cores GeoB16224-1,[103] CDH86,[102] GL-1248,[105] GeoB3910-2,[101] and M125-95-3[104] (Figure S1). (B) Comparison between stacked cave and Greenland ice-core records. (a) DO-1–13 stack of NGRIP ice-core $\delta^{18}O$,[29] (b) DO-8 (HS4) and DO-12 (HS5) onset (termination) stack of NGRIP ice-core $\delta^{18}O$.[27] (c) and (d) Stacked cave $\delta^{18}O$ records incorporating the HS2, HS4 and HS5 terminations (or DO-2，DO-8 and DO-12 onsets) from caves in the ASM and SASM domains, respectively (see Text S5 & Data S4). The vertical orange dashed line indicates the onset of abrupt transition in different records, and the vertical grey dashed line in (d) indicates the end of the transition. Shaded areas indicate ±1σ error ranges.

value and variability.[33,47] Overall, the age uncertainty of ASM-2026 is relatively small (Figure 1), and particularly, the Hulu Cave speleothems that make up the major part of ASM-2026 show an almost constant growth rate (Figure S3), which facilitates the high frequency analysis. The spectral analyses of ASM-2026 time series show a pattern broadly similar to NGRIP, with lower-amplitude (~0.25 ‰) and shorter-periodicity (~30-year) variability during the Holocene compared to the last glacial (~0.5 ‰ amplitude and ~200–30-year periodicity) (Figures 6A & S20A-B). Taken together, Greenland ice-core and ASM-2026 records indicate a pattern of lower amplitude and shorter periodicities during warmer conditions (the Holocene) compared to the last glacial period. This coherence aligns with model studies suggesting that variations in the AMOC on the same timescales delimit these patterns.[110] As such, it is likely that Greenland temperatures and ASM dynamics are largely coordinated by AMOC changes at multidecadal-centennial scales as suggested by recent studies (e.g., refs.[29,111,112]). It should be noted that the ASM-2026 record involves the splicing of multiple cave speleothem records, which may affect the analyses of interdecadal variability. Therefore, these results await further validation.

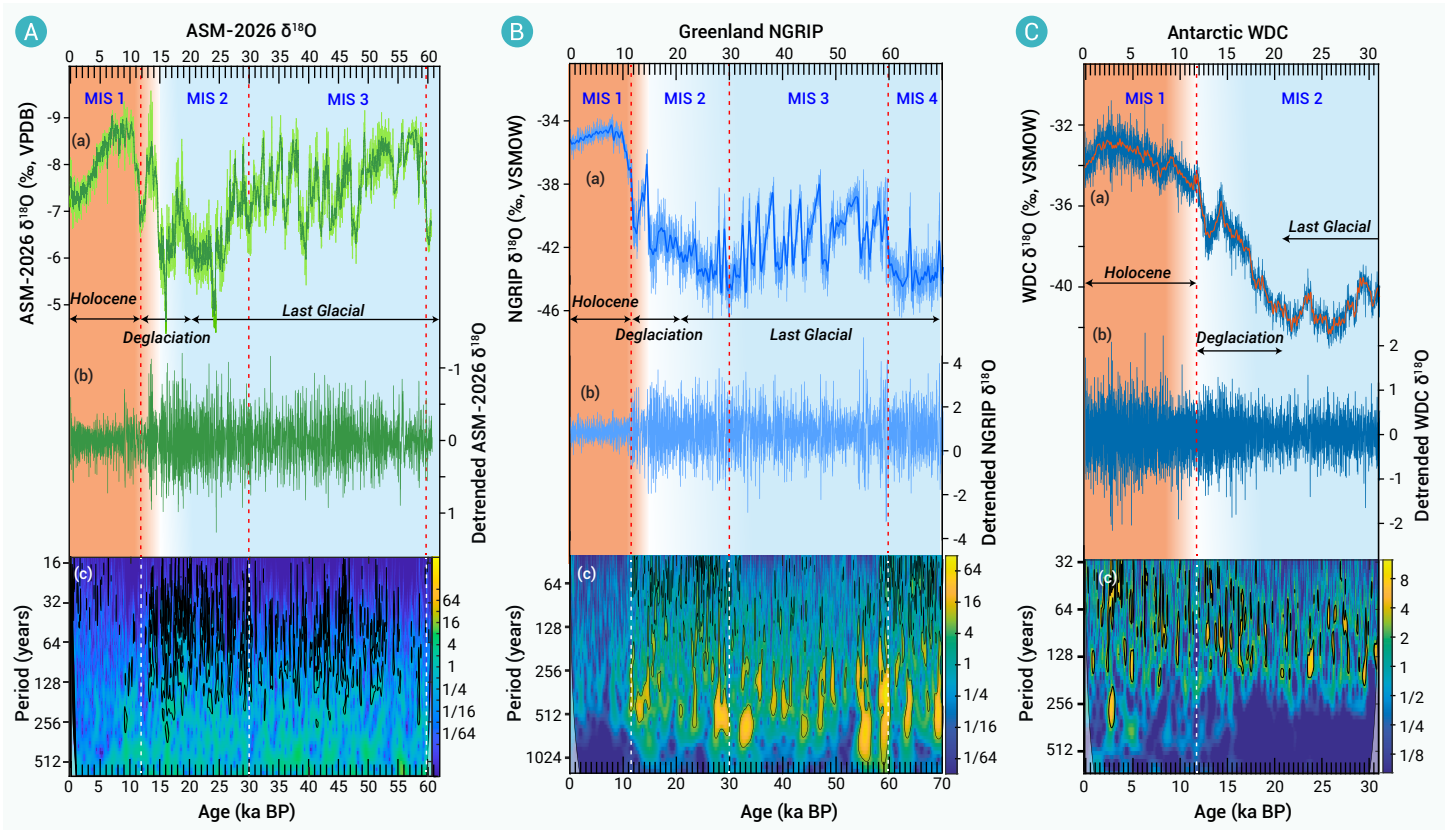

Figure 6. Climate variability across the last 60 ka (A) shows the ASM variability over the last 60 ka: (a) ASM-2026 record (light green, this study) and its low-frequency signal (dark green) obtained using the Ensemble Empirical Mode Decomposition (EEMD) method.[113] (b) High-frequency signals in the ASM-2026 record after removal of the low-frequency signals. (c) Wavelet analysis of the ASM-2026 record using the MATLAB wavelet coherence package. Spectral power (variance) is represented by blue (weak) to yellow (strong) colors. Black lines indicate the 95% significance level and the cone of influence.[114] Vertical dashed lines depict the time ranges of Marine Isotope Stage (MIS) 1, 2, and 3. Colors approximately depict the Holocene (pumpkin), deglacial (white), and last glacial (light blue) periods. (B) is similar to (A) but for Greenland temperature variability. (a)-(c) are similar to those in (A) but for the NGRIP $\delta^{18}O$ record[2,61] with adjusted chronology to XJTU-1.0. Panel (C) is similar to (A) but for Antarctic temperature variability over the last 31 ka. (a)-(c) are similar to those in (A) but for the Antarctic WDC $\delta^{18}O$ record[23] with chronology adjusted to XJTU-1.0.

Among Antarctic ice cores, the WDC $\delta^{18}O$ record stands out not only for its high resolution, which is attributed to its high snow accumulation rate, but also its excellent chronology, which is based on annual layer counting for the last 31.2 ka.[115] While uncertainties remain regarding diffusion and post-formation changes, their impact on multidecadal to centennial variability analysis is minimal, particularly for the last 30 ka, where such effects are on the order of a few years.[116] In contrast to Greenland and ASM $\delta^{18}O$ records, the WDC $\delta^{18}O$ shows an opposite pattern. During the last glacial period, it shows a smaller amplitude variation (~0.5‰) compared to larger amplitude variations (~1‰) during the Holocene. However, its periodicities from the last glacial to the Holocene appear to be comparable or slightly longer (rather than shorter) (Figures 6 & S20C). This suggests different interhemispheric teleconnections under glacial and interglacial conditions. During the glacial period, NH forcing dominated globally, resulting in a north-to-south directionality in the amplitudes of multidecadal to centennial variability. Conversely, during the interglacial (the Holocene) period, Antarctic ice-sheet dynamics, inferred from indicators like iceberg-rafted debris, might have driven hydroclimate fluctuations, resulting in larger amplitudes of decadal to centennial variability.[117–121] Nonetheless, the question of whether the significantly larger Antarctic hydroclimate fluctuations during the Holocene had a widespread or even global impact remains open. This calls for more empirical and model studies in future.

CONCLUSION

The new composite high-resolution and precisely dated cave $\delta^{18}O$ record, ASM-2026, characterizes the ASM dynamic variability over the last 60 ka. The chronological framework of ASM-2026 (XJTU-1.0) is consistent within uncertainties with the NGRIP ice core-based GICC05 chronology, but offers significantly more precise age benchmarks for calibrating and correlating global climate variability, thus facilitating the establishment of a "Paleoclimatic Rosetta Stone". Within this climatic correlation framework, ASM dynamics are largely independent of northern and southern high-latitude ice-sheet forcings from glacial-interglacial to millennial timescales, but are closely coupled with AMOC variations on a wide range of sub-orbital timescales. Our study reinforces the notion that terminations, specifically HSs, commenced with a centennial-scale weakening of the SAM, likely linked to the SH shift from AAO+ to AAO– mode near the end of HSs. This suggests a more active role of low-latitude and SH hydroclimate changes, either as triggers, as critical positive feedbacks, or both. The most prominent millennial cycle is centered at ~4.5-ka, and its trigger may be linked to the equatorial insolation, thus residing in low-latitude regimes. On multidecadal to centennial timescales, the periodicity and amplitude of the ASM and Greenland climate variabilities decreased from glacial to interglacial, in contrast to the Antarctic climate variability, suggesting changes in climate drivers and/or in their directionality across the glacial-interglacial conditions.

REFERENCES

1. Dansgaard W., Johnsen S.J., Clausen H.B. et al. (1993). Evidence for general instability of past climate from a 250-kyr ice-core record. *Nature* **364**:218–220. DOI:10.1038/364218a0
2. Rasmussen S.O., Bigler M., Blockley S.P. et al. (2014). A stratigraphic framework for abrupt climatic changes during the last glacial period based on three synchronized Greenland ice-core records: Refining and extending the INTIMATE event stratigraphy. *Quat. Sci. Rev.* **106**:14–28. DOI:10.1016/j.quascirev.2014.09.007
3. Heinrich H. (1988). Origin and consequences of cyclic ice rafting in the northeast Atlantic Ocean during the past 130,000 years. *Quat. Res.* **29**:142–152. DOI:10.1016/0033-5894(88)90057-9
4. Hemming S.R. (2004). Heinrich events: Massive late Pleistocene detritus layers of the North Atlantic and their global climate imprint. *Rev. Geophys.* **42**:RG1005. DOI:10.1029/2003rg000128
5. Barker S., Diz P., Vautravers M.J. et al. (2009). Interhemispheric Atlantic seesaw response during the last deglaciation. *Nature* **457**:1097–1102. DOI:10.1038/

nature07770
6. Hodell D.A., Nicholl J.A., Bontognali T.R.R. et al. (2017). Anatomy of Heinrich Layer 1 and its role in the last deglaciation. *Paleoceanography* **32**:284–303. DOI:10.1002/2016pa003028
7. Dong X.Y., Kathayat G., Rasmussen S.O. et al. (2022). Coupled atmosphere-ice-ocean dynamics during Heinrich Stadial 2. *Nat. Commun.* **13**:5867. DOI:10.1038/s41467-022-33583-4
8. Cheng H., Fleitmann D., Edwards R.L. et al. (2009). Timing and structure of the 8.2 kyr BP event inferred from $\delta^{18}O$ records of stalagmites from China, Oman, and Brazil. *Geology* **37**:1007–1010. DOI:10.1130/g30126a.1
9. Cheng H., Zhang H.W., Spötl C. et al. (2020). Timing and structure of the Younger Dryas event and its underlying climate dynamics. *Proc. Natl. Acad. Sci. USA* **117**:23408–23417. DOI:10.1073/pnas.2007869117
10. Menviel L.C., Skinner L.C., Tarasov L. et al. (2020). An ice-climate oscillatory framework for Dansgaard-Oeschger cycles. *Nat. Rev. Earth Environ.* **1**:677–693. DOI:10.1038/s43017-020-00106-y
11. Broccoli A.J., Dahl K.A., Stouffer R.J. et al. (2006). Response of the ITCZ to Northern Hemisphere cooling. *Geophys. Res. Lett.* **33**:L01702. DOI:10.1029/2005gl024546
12. Deplazes G., Lückge A., Peterson L.C. et al. (2013). Links between tropical rainfall and North Atlantic climate during the last glacial period. *Nat. Geosci.* **6**:213–217. DOI:10.1038/ngeo1712
13. Chiang J.C.H., Fung I.Y., Wu C.H. et al. (2015). Role of seasonal transitions and westerly jets in East Asian paleoclimate. *Quat. Sci. Rev.* **108**:111–129. DOI:10.1016/j.quascirev.2014.11.009
14. Cheng H., Edwards R.L., Wang Y.J. et al. (2006). A penultimate glacial monsoon record from Hulu Cave and two-phase glacial terminations. *Geology* **34**:217–220. DOI:10.1130/g22289.1
15. Cheng H., Xu Y., Dong X.Y. et al. (2021). Onset and termination of Heinrich Stadial 4 and the underlying climate dynamics. *Commun. Earth Environ.* **2**:230. DOI:10.1038/s43247-021-00304-6
16. Dong X.Y., Zhang X., Zhang H.W. et al. (2025). Interstadial diversity of East Asian summer monsoon linked to changes of the Northern Westerlies. *Nat. Commun.* **16**:7765. DOI:10.1038/s41467-025-63057-2
17. Cheng H., Sinha A., Cruz Jr F.W. et al. (2013). Climate change patterns in Amazonia and biodiversity. *Nat. Commun.* **4**:1411. DOI:10.1038/ncomms2415
18. Cruz Jr F.W., Burns S.J., Karmann I. et al. (2005). Insolation-driven changes in atmospheric circulation over the past 116,000 years in subtropical Brazil. *Nature* **434**:63–66. DOI:10.1038/nature03365
19. Leduc G., Vidal L., Tachikawa K. et al. (2007). Moisture transport across Central America as a positive feedback on abrupt climatic changes. *Nature* **445**:908–911. DOI:10.1038/nature05578
20. Wang X.F., Auler A.S., Edwards R.L. et al. (2004). Wet periods in northeastern Brazil over the past 210 kyr linked to distant climate anomalies. *Nature* **432**:740–743. DOI:10.1038/nature03067
21. Wang X.F., Edwards R.L., Auler A.S. et al. (2017). Hydroclimate changes across the Amazon lowlands over the past 45,000 years. *Nature* **541**:204–207. DOI:10.1038/nature20787
22. Pedro J.B., Jochum M., Buizert C. et al. (2018). Beyond the bipolar seesaw: Toward a process understanding of interhemispheric coupling. *Quat. Sci. Rev.* **192**:27–46. DOI:10.1016/j.quascirev.2018.05.005
23. Brook E. J. and Buizert C. (2018). Antarctic and global climate history viewed from ice cores. *Nature* **558**:200–208. DOI:10.1038/s41586-018-0172-5
24. Buizert C., Sigl M., Severi M. et al. (2018). Abrupt ice-age shifts in southern westerly winds and Antarctic climate forced from the north. *Nature* **563**:681–685. DOI:10.1038/s41586-018-0727-5
25. Wendt K.A., Nehrbass-Ahles C., Niezgoda K. et al. (2024). Southern Ocean drives multidecadal atmospheric CO_2 rise during Heinrich Stadials. *Proc. Natl. Acad. Sci. USA* **121**:e2319652121. DOI:10.1073/pnas.2319652121
26. Stocker T.F. and Johnsen S.J. (2003). A minimum thermodynamic model for the bipolar seesaw. *Paleoceanogr. Paleoclimatol.* **18**:1087–1088. DOI:10.1029/2003pa000920
27. WAIS Divide Project Members. (2015). Precise interpolar phasing of abrupt climate change during the last ice age. *Nature* **520**:661–665. DOI:10.1038/nature14401
28. Svensson A., Dahl-Jensen D., Steffensen J.P. et al. (2020). Bipolar volcanic synchronization of abrupt climate change in Greenland and Antarctic ice cores during the last glacial period. *Clim. Past* **16**:1565–1580. DOI:10.5194/cp-16-1565-2020
29. Dong X.Y., Zhang X., Sun Y.C. et al. (2026). Glacial abrupt transitions in ocean circulation were much slower than ice-core records imply. *Science* (in review).
30. Cheng H., Edwards R.L., Shen C.-C. et al. (2013). Improvements in ^{230}Th dating, ^{230}Th and ^{234}U half-life values, and U-Th isotopic measurements by multi-collector inductively coupled plasma mass spectrometry. *Earth Planet. Sci. Lett.* **371–372**:82–91. DOI:10.1016/j.epsl.2013.04.006
31. Cheng H., Edwards R.L., Broecker W.S. et al. (2009). Ice age terminations. *Science* **326**:248–252. DOI:10.1126/science.1177840
32. Zhao J.Y., Pérez - Mejías C., Dong X.Y. et al (2025). Resonant Asian monsoon during intermediate conditions of the last deglaciation: Insights from speleothem records. *J. Geophys. Res. Atmos.* **130**:e2024JD042523. DOI:10.1029/2024JD042523
33. Cheng H., Edwards R.L., Sinha A. et al. (2016). The Asian monsoon over the past 640,000 years and ice age terminations. *Nature* **534**:640–646. DOI:10.1038/nature18591
34. Cheng H., Li H.Y., Sha L.J. et al. (2022). Milankovitch theory and monsoon. *The Innovation* **3**:100338. DOI:10.1016/j.xinn.2022.100338
35. Sinha A., Cheng J., Li H.Y. et al. (2026). ENSO modulated upstream convection as the primary control on interannual $\delta^{18}O$ variability in East Asia. *npj Clim. Atmos. Sci.* **9**:64. DOI:10.1038/s41612-026-01333-8
36. Edwards R.L., Chen J.H., Wasserburg G.J. (1987). ^{238}U-^{234}U-^{230}Th-^{232}Th systematics and the precise measurement of time over the past 500,000 years. *Earth Planet. Sci. Lett.* **81**:175–192. DOI:10.1016/0012-821x(87)90154-3
37. Cheng H., Edwards R.L., Hoff J. et al. (2000). The half-lives of uranium-234 and thorium-230. *Chem. Geol.* **169**:17–33. DOI:10.1016/S0009-2541(99)00157-6
38. Scholz D. and Hoffmann D.L. (2011). StalAge - An algorithm designed for construction of speleothem age models. *Quat. Geochron.* **6**:369–382. DOI:10.1016/j.quageo.2011.02.002
39. Ramsey C.B. (2009). Deposition models for chronological records. *Quat. Sci. Rev.* **27**:42–60. DOI:10.1016/j.quascirev.2007.01.019
40. Cheng H., Edwards R.L., Southon J. et al. (2018). Atmospheric $^{14}C/^{12}C$ changes during the last glacial period from Hulu Cave. *Science* **362**:1293–1297. DOI:10.1126/science.aau0747
41. Wang Y.J., Cheng H., Edwards R.L. et al. (2005). The Holocene Asian monsoon: links to solar changes and North Atlantic climate. *Science* **308**:854–857. DOI:10.1126/science.1106296
42. Dykoski C.A., Edwards R.L., Cheng H. et al. (2005). A high-resolution, absolute-dated Holocene and deglacial Asian monsoon record from Dongge Cave, China. *Earth Planet. Sci. Lett.* **233**:71–86. DOI:10.1016/j.epsl.2005.01.036
43. Zhang W.H., Wu J.Y., Wang Y.J. et al. (2014). A detailed East Asian monsoon history surrounding the "Mystery Interval" derived from three Chinese speleothem records. *Quat. Res.* **82**:154–163. DOI:10.1016/j.yqres.2014.01.010
44. Liu D.B., Wang Y.J., Cheng H. et al (2010). Sub-millennial variability of Asian monsoon intensity during the early MIS 3 and its analogue to the ice age terminations. *Quat. Sci. Rev.* **29**:1107–1115. DOI:10.1016/j.quascirev.2010.01.008
45. Wang Y.J., Cheng H., Edwards R.L. et al. (2001). A high-resolution absolute-dated late Pleistocene monsoon record from Hulu Cave, China. *Science* **294**:2345–2348. DOI:10.1126/science.1064618
46. Zhao K., Wulder M.A., Hu T.X. et al. (2019). Detecting change-point, trend, and seasonality in satellite time series data to track abrupt changes and nonlinear dynamics: A Bayesian ensemble algorithm. *Remote Sens. Environ.* **232**:111181. DOI:10.1016/j.rse.2019.04.034
47. Yuan D.X., Cheng H., Edwards R.L. et al. (2004). Timing, duration, and transitions of the last interglacial Asian monsoon. *Science* **304**:575–578. DOI:10.1126/science.1091220
48. Li Y., Qiu W.Y., Gao K. et al. (2025) Millennial-scale East Asian summer monsoon hydroclimate variability during 47–39 kyr B.P. inferred from a stalagmite IRMsoft-flux record in Southeastern China. *Global Planet. Change* **253**: 104954. DOI:10.1016/j.gloplacha.2025.104954
49. Wang Y.J., Cheng H., Edwards R.L. et al. (2008). Millennial- and orbital-scale changes in the East Asian monsoon over the past 224,000 years. *Nature* **451**:1090–1093. DOI:10.1038/nature06692
50. Buizert C., Cuffey K.M., Severinghaus J.P. et al. (2015). The WAIS divide deep ice core WD2014 chronology - part 1: Methane synchronization (68-31 ka BP) and the gas age-ice age difference. *Clim. Past* **11**:153–173. DOI:10.5194/cp-11-153-2015
51. Corrick E.C., Drysdale R.N., Hellstrom J.C. et al. (2020). Synchronous timing of abrupt climate changes during the last glacial period. *Science* **369**:963–969. DOI:10.1126/science.aay5538
52. Liu D.B., Mi X., Liu S.S. et al. (2022). Multi-phased Asian hydroclimate variability during Heinrich Stadial 5. *Clim. Dyn.* **60**:4003–4016. DOI:10.1007/s00382-022-06566-w
53. Du W.J., Cheng H., Xu Y. et al. (2019). Timing and structure of the weak Asian Monsoon event about 73,000 years ago. *Quat. Geochron.* **53**:101003. DOI:10.1016/j.quageo.2019.05.002
54. Waelbroeck C., Lougheed B.C., Vázquez Riveiros N. et al. (2019). Consistently dated Atlantic sediment cores over the last 40 thousand years. *Sci. Data* **6**:165. DOI:10.1038/s41597-019-0173-8
55. Andersen K.K., Svensson A., Johnsen S.J. et al. (2006). The greenland ice core chronology 2005, 15-42 ka. part 1: Constructing the time scale. *Quat. Sci. Rev.* **25**:3246–3257. DOI:10.1016/j.quascirev.2006.08.002.
56. Rasmussen S.O., Andersen K.K., Svensson A.M. et al. (2006). A new Greenland ice core chronology for the last glacial termination. *J. Geophys. Res. Atmospheres* **111**:D06102. DOI:10.1029/2005JD006079
57. Svensson A., Andersen K.K., Bigler M. et al. (2006). The greenland ice core chronology 2005, 15-42 ka. part 2: comparison to other records. *Quat. Sci. Rev.* **25**:3258–3267. DOI:10.1016/j.quascirev.2006.08.003
58. Svensson A., Andersson K.K., Bigler M. et al. (2008). A 60,000 year Greenland stratigraphic ice core chronology. *Clim. Past* **4**:47–57. DOI:10.5194/cp-4-47-2008
59. An Z.S., Kukla G.J., Porter S.C. et al. (1991) Magnetic susceptibility evidence of monsoon variation on the Loess Plateau of central China during the last 130,000

years. *Quat. Res.* **36**:29-36. DOI:10.1016/0033-5894(91)90015-W
60. Laskar J., Robutel P., Joutel F. et al. (2004). A long-term numerical solution for the insolation quantities of the Earth. *Astron. Astrophys.* **428**:261–285. DOI:10.1051/0004-6361:20041335
61. North Greenland Ice Core Project members. (2004). High-resolution record of Northern Hemisphere climate extending into the last interglacial period. *Nature* **431**:147–151. DOI:10.1038/nature02805
62. Böhm E., Lippold J., Gutjahr M. et al. (2015). Strong and deep Atlantic Meridional Overturning Circulation during the last glacial cycle. *Nature* **517**:73–76. DOI:10.1038/nature14059
63. Henry L.G., McManus J.F., Curry W.B. et al. (2016). North Atlantic Ocean circulation and abrupt climate change during the last glaciation. *Science* **353**:470–474. DOI:10.1126/science.aaf5529
64. Toucanne S., Soulet G., Vázquez Riveiros N. et al. (2021). The North Atlantic glacial rastern boundary current as a key driver for ice-sheet—AMOC interactions and climate instability. *Paleoceanogr. Paleoclimatol.* **36**:e2020PA004068. DOI:10.1029/2020pa004068
65. Davtian N. and Bard E. (2023). A new view on abrupt climate changes and the bipolar seesaw based on paleotemperatures from Iberian Margin sediments. *Proc. Natl. Acad. Sci. USA* **120**:e2209558120. DOI:10.1073/pnas.2209558120
66. Siddall M., Rohling E.J., Almogi-Labin A. et al. (2003). Sea-level fluctuations during the last glacial cycle. *Nature* **423**:853–858. DOI:10.1038/nature01690
67. Margari V., Skinner L.C., Menviel L. et al. (2020). Fast and slow components of interstadial warming in the North Atlantic during the last glacial. *Commun. Earth Environ.* **1**:6. DOI:10.1038/s43247-020-0006-x
68. Rhodes R.H., Brook E.J., Chiang J.C.H. et al. (2015). Enhanced tropical methane production in response to iceberg discharge in the North Atlantic. *Science* **348**:1016–1019. DOI:10.1126/science.1262005
69. Bauska T.K., Marcott S.A., Brook E.J. et al. (2021). Abrupt changes in the global carbon cycle during the last glacial period. *Nat. Geosci.* **14**:91–96. DOI:10.1038/s41561-020-00680-2
70. Mosblech N., Bush M., Gosling W. et al. (2012). North Atlantic forcing of Amazonian precipitation during the last ice age. *Nat. Geosci.* **5**:817–820. DOI:10.1038/ngeo1588
71. Martin K., Buizert C., Edwards J. et al. (2023). Bipolar impact and phasing of Heinrich-type climate variability. *Nature* **617**:1–5. DOI:10.1038/s41586-023-05875-2
72. Muschitiello F. and Aquino-Lopez M.A. (2024). Continuous synchronization of the Greenland ice-core and U–Th timescales using probabilistic inversion. *Clim. Past* **20**:1415–1435. DOI:10.5194/cp-20-1415-2024
73. Hodell D.A., Crowhurst S.J., Lourens L. et al. (2023). A 1.5-million-year record of orbital and millennial climate variability in the North Atlantic. *Clim. Past* **19**:607–636. DOI:10.5194/cp-19-607-2023
74. Wolff E. W., Fischer H., Röthlisberger R. et al. (2009). Glacial terminations as southern warmings without northern control. *Nat. Geosci.* **2**:206–209. DOI:10.1038/ngeo442
75. Cai Y.J., An Z.S., Cheng H. et al. (2006). High-resolution absolute-dated Indian Monsoon record between 53 and 36 ka from Xiaobailong Cave, southwestern China. *Geology* **34**:621–624. DOI:10.1130/g22567
76. Rohling E.J., Liu Q.S., Roberts A.P. et al. (2009). Controls on the East Asian monsoon during the last glacial cycle, based on comparison between Hulu Cave and polar ice-core records. *Quat. Sci. Rev.* **28**:3291–3302. DOI:10.1016/j.quascirev.2009.09.007
77. An Z.S., Clemens S.C., Shen J. et al. (2011). Glacial-interglacial Indian summer monsoon dynamics. *Science* **333**:719–723. DOI:10.1126/science.1203752
78. Chen X., Zhao J.Y., Wang K.X. et al. (2025). Nonlinear feedback of Asian summer monsoon to abrupt events in North Atlantic: Evidence from a precisely dated speleothem record during late MIS3. *Global Planet. Change* **247**:104733. DOI:10.1016/j.gloplacha.2025.104733
79. Svensson, A., Vettoretti G., Lin J.M. et al. (2026) Bipolar volcanic ice-core synchronization of the entire last glacial period. *Quat. Sci. Rev.* **375**:109755. DOI:10.1016/j.quascirev.2025.109755
80. Pollard D. and DeConto R.M. (2009). Modelling West Antarctic ice sheet growth and collapse through the past five million years. *Nature* **458**:329–333. DOI:10.1038/nature07809
81. Gottschalk J., Skinner L.C., Jaccard S.L. et al. (2020). Southern Ocean link between changes in atmospheric CO_2 levels and northern-hemisphere climate anomalies during the last two glacial periods. *Quat. Sci. Rev.* **230**:106067. DOI:10.1016/j.quascirev.2019.106067
82. Menviel L. and Spence P. (2024). Southern Ocean circulation's impact on atmospheric CO_2 concentration. *Front. Mar. Sci.* **10**:1328534. DOI:10.3389/fmars.2023.1328534
83. Markle B.R., Steig E.J., Buizert C. et al. (2017). Global atmospheric teleconnections during Dansgaard-Oeschger events. *Nat. Geosci.* **10**:36–40. DOI:10.1038/ngeo2848
84. Zhang R. and Delworth T.L. (2005). Simulated tropical response to a substantial weakening of the Atlantic thermohaline circulation. *J. Clim.* **18**:1853–1860. DOI:10.1175/jcli3460.1
85. Erhardt T., Capron E., Rasmussen S.O. et al. (2019). Decadal-scale progression of the onset of Dansgaard–Oeschger warming events. *Clim. Past* **15**:811–825. DOI:10.5194/cp-15-811-2019
86. He C.F., Liu Z.Y., Otto-Bliesner B.L. et al. (2021). Abrupt Heinrich Stadial 1 cooling missing in Greenland oxygen isotopes. *Sci. Adv.* **7**:eabh1007. DOI:10.1126/sciadv.abh1007
87. Yu T., Cheng J., Lin P. et al. (2018). Responses and mechanisms of East Asian winter and summer monsoons to weakened Atlantic meridional overturning circulation using the FGOALS-g2 model. *Int. J. Clim.* **38**:2618–2626. DOI:10.1002/joc.5373
88. Manabe S. and Stouffer R. (1997). Coupled ocean-atmosphere model response to freshwater input: Comparison to Younger Dryas Event. *Paleoceanography* **12**:321–336. DOI:10.1029/96pa03932
89. Otto-Bliesner B. and Brady E. (2010). Sensitivity of the climate response to the magnitude and location of freshwater forcing: Last glacial maximum experiments. *Quat. Sci. Rev.* **29**:56–73. DOI:10.1016/j.quascirev.2009.07.004
90. Rahmstorf S. (2002). Ocean circulation and climate during the past 120,000 years. *Nature* **419**:207–214. DOI:10.1038/nature01090
91. Scafetta N., Milani F., Bianchini A. et al. (2016). On the astronomical origin of the Hallstatt oscillation found in radiocarbon and climate records throughout the Holocene. *Earth Sci. Rev.* **162**:24–43. DOI:10.1016/j.earscirev.2016.09.004
92. Keigwin L.D. and Jones G.A. (1994). Western North Atlantic evidence for millennial-scale changes in ocean circulation and climate. *J. Geophys. Res. -Oceans* **99**:12397–12410. DOI:10.1029/94jc00525
93. Weirauch D. and Billups K., Martin P. (2008). Evolution of millennial-scale climate variability during the mid Pleistocene. *Paleoceanography* **23**:PA3216. DOI:10.1029/2007pa001584
94. Billups K. and Scheinwald A. (2014). Origin of millennial-scale climate signals in the subtropical North Atlantic. *Paleoceanography* **29**:612–627. DOI:10.1002/2014pa002641
95. Kravchinsky V.A., Zhang R., Borowiecki R. et al. (2025). Millennial cycles in Greenland and Antarctic ice core records: Evidence of astronomical influence on global climate. *J. Geophys. Res.-Atmos.* **130**:e2024JD042810. DOI:10.1029/2024JD042810
96. Gorbarenko S.A., Harada N., Malakhov M.I. et al. (2012). Responses of the Okhotsk Sea environment and sedimentology to global climate changes at the orbital and millennial scale during the last 350 kyr. *Deep Sea Res. Part II Top. Stud. Oceanogr.* **61**:73–84. DOI:10.1016/j.dsr2.2011.05.016
97. Zhang X., Barker S., Knorr G. et al. (2021). Direct astronomical influence on abrupt climate variability. *Nat. Geosci.* **14**:819–826. DOI:10.1038/s41561-021-00846-6
98. Niu X.W., Wang J., Kang L. et al. (2025). Millennial-scale climate variability of the Asian summer monsoon over the last 690,000 years: Insights from cave records. *Sci. Bull.* **70**:1513–1522. DOI:10.1016/j.scib.2025.02.011
99. Zhang Z.F., Huang Y.J., Wang T.T. et al. (2025). Precession-induced millennial climate cycles in greenhouse Cretaceous. *Nat. Commun.* **16**:10696. DOI:10.1038/s41467-025-66219-4
100. Berger A., Loutre M.F., Mélice J.L. et al. (2006). Equatorial insolation: From precession harmonics to eccentricity frequencies. *Clim. Past* **2**:519–533. DOI:10.5194/cp-2-131-2006,2006
101. Jaeschke A., Rühlemann C., Arz H. et al. (2007). Coupling of millennial-scale changes in sea surface temperature and precipitation off northeastern Brazil with high-latitude climate shifts during the last glacial period. *Paleoceanography* **22**:PA4206. DOI:10.1029/2006pa001391
102. Nace T.E., Baker P.A., Dwyer G.S. et al. (2014). The role of North Brazil Current transport in the paleoclimate of the Brazilian Nordeste margin and paleoceanography of the western tropical Atlantic during the late Quaternary. *Palaeogeogr. Palaeoclimatol. Palaeoecol.* **415**:3–13. DOI:10.1016/j.palaeo.2014.05.030
103. Zhang Y., Chiessi C.M., Mulitza S. et al. (2017). Different precipitation patterns across tropical South America during Heinrich and Dansgaard-Oeschger stadials. *Quat. Sci. Rev.* **177**:1–9. DOI:10.1016/j.quascirev.2017.10.012
104. Campos M.C., Chiessi C.M., Prange M. et al. (2019). A new mechanism for millennial scale positive precipitation anomalies over tropical South America. *Quat. Sci. Rev.* **225**:105990. DOI:10.1016/j.quascirev.2019.105990
105. Venancio I.M., Shimizu M.H., Santos T.P. et al. (2020). Changes in surface hydrography at the western tropical Atlantic during the Younger Dryas. *Global Planet. Change* **184**:103047. DOI:10.1016/j.gloplacha.2019.103047
106. Venancio I.M., Nascimento R.A., Santos T.P. et al. (2022). Tropical South American rainfall response to Dansgaard-Oeschger Stadials of Marine Isotope Stage 5. *Front. Earth Sci.* **10**:826993. DOI:10.3389/feart.2022.826993
107. Thompson D.W.J. and Wallace J.M. (2000). Annular modes in the extratropical circulation. Part I: month-to-month variability. *J. Clim.* **13**:1000–1016. DOI:10.1175/1520-0442(2000)013<1000:AMITEC>2.0.CO;2
108. Gong D. and Wang S. (1998). Antarctic oscillation: concept and applications. *Sci. Bull.* **43**:734–738. DOI:10.1007/bf02898949
109. Gkinis V., Simonsen S.B., Buchardt S.L. et al. (2014). Water isotope diffusion rates from the NorthGRIP ice core for the last 16,000 years—Glaciological and paleoclimatic implications. *Earth Planet. Sci. Lett.* **405**:132–141. DOI:10.1016/j.epsl.2014.08.022
110. Cheng J., Liu Z.Y., Zhang S.Q. et al. (2016). Reduced interdecadal variability of Atlantic Meridional Overturning Circulation under global warming. *Proc. Natl. Acad. Sci. USA* **113**:3175–3178. DOI:10.1073/pnas.1519827113
111. Zhao J.Y., Cheng H., Cao J. et al. (2023). Orchestrated decline of Asian summer

monsoon and Atlantic meridional overturning circulation in global warming period. *Innov. Geosci.* **1**:100011. DOI:10.59717/j.xinn-geo.2023.100011
112. Wang K.X., Zhao J.Y., Wang J.J. et al. (2024). Past decadal climate variability of East Asian summer monsoon: Characteristics and mechanisms (in Chinese). *Chin. Sci. Bull.* **70**:240–261. DOI:10.1360/tb-2024-0161
113. Wu Z. and Huang N.E. (2009). Ensemble empirical mode decomposition: A noise-assisted data analysis method. *Adv. Adapt. Data Anal.* **1**:1–41. DOI:10.1142/s1793536909000047
114. Grinsted A., Moore J.C., Jevrejeva S. et al. (2004). Application of the cross wavelet transform and wavelet coherence to geophysical time series. *Nonlinear Proc. Geophys.* **11**:561–566. DOI:10.5194/npg-11-561-2004
115. Sigl M., Fudge T.J., Winstrup M. et al. (2016). The WAIS Divide deep ice core WD2014 chronology - Part 2: Annual-layer counting (0-31 ka BP). *Clim. Past* **12**:769–786. DOI:10.5194/cp-12-769-2016
116. Jones T.R., Roberts W.H.G., Steig E.J. et al. (2018). Southern Hemisphere climate variability forced by Northern Hemisphere ice-sheet topography. *Nature* **554**:351–355. DOI:10.1038/nature24669
117. Weber M.E., Clark P.U., Kuhn G. et al. (2014). Millennial-scale variability in Antarctic ice-sheet discharge during the last deglaciation. *Nature* **510**:134–138. DOI:10.1038/nature13397
118. Bakker P., Clark P.U., Golledge N.R. et al. (2016). Iceberg-rafted debris stack of sediment cores MD07-3133 and MD07-3134, 0-10 ka (dataset). *PANGAEA*. DOI: 10.1594/PANGAEA.865349
119. Bakker P., Clark P.U., Golledge N.R. et al. (2017). Centennial-scale Holocene climate variations amplified by Antarctic Ice Sheet discharge. *Nature* **541**:72–76. DOI:10.1038/nature20582
120. Noble T.L., Rohling E.J., Aitken A.R.A. et al. (2020). The sensitivity of the Antarctic Ice Sheet to a changing climate: past, present, and future. *Rev. Geophys.* **58**:e2019RG000663. DOI:10.1029/2019rg000663
121. Weber M.E., Golledge N.R., Fogwill C.J. et al. (2021). Decadal-scale onset and termination of Antarctic ice-mass loss during the last deglaciation. *Nat. Commun.* **12**:6683. DOI:10.1038/s41467-021-27053-6

FUNDING AND ACKNOWLEDGMENTS

The authors wish to thank Sune O. Rasmussen and Anders Svensson for helpful discussions. This work was supported by the National Natural Science Foundation of China (NSFC) grants (42488201 to H.C.), Xi'an Jiaotong University special fund for discipline development in global environmental change science (key project) (H.C.), the grant of State Key Laboratory of Loess Science (SKLLQGZR2401 to H.C.), the NSFC grants (423B2204 to X.D., 425B2016 to X.N. and 42102229 to H.L.), the China Postdoctoral Science Foundation under Grant Number 2025M780387 (X.D.), and the fundamental research funding for free exploration and innovation projects at Xi'an Jiaotong University under Grant Number xzy012026038 (X.D.). The funders had no role in study design, data collection and analysis, decision to publish, or preparation of the manuscript.

AUTHOR CONTRIBUTIONS

H.C. conceptualized this study. X.D., B.Z. and X.J. conducted experiments. X.D., H.L., X.N., J.Z. conducted data analyses. H.C. wrote the initial draft. H.C., X.D., H.L, X.N., A.S., Y.C., H.Z., C.S. made revisions. All authors contributed to the manuscript and approved the final version.

DECLARATION OF INTERESTS

Hai Cheng, Ashish Sinha, Haiwei Zhang, Francisco W. Cruz and Christoph Spötl are editorial board members/associate editors of *The Innovation Geoscience* and were blinded from reviewing or making final decisions on the manuscript. Peer review was handled independently of these members and their research groups. The other authors declare no conflicts of interest.

DATA AND CODE AVAILABILITY

The data are openly available in the supplementary materials accompanying this manuscript.

SUPPLEMENTAL INFORMATION

It can be found online at https://doi.org/10.59717/j.xinn-geo.2026.100243.

LEAD CONTACT WEBSITE

Hai Cheng: http://gr.xjtu.edu.cn/web/cheng021